doi: 10.1016/j.ccr.2015.07.001

The Anderson-Evans polyoxometalate: From inorganic building blocks *via* hybrid organic-inorganic structures to tomorrows “Bio-POM”

Amir Blazevic, Annette Rompel*

Institut für Biophysikalische Chemie, Fakultät für Chemie, Universität Wien, Althanstraße 14, 1090 Wien, Austria

* e-mail: annette.rompel@univie.ac.at, phone: +43-1-4277-525 02, www.bpc.univie.ac.at

Keywords: Anderson-Evans POM, synthetic strategy, hybrid organic-inorganic, tris-functionalization, POM-protein interaction

Abstract

One of the most common polyoxometalates (POMs) is the Anderson-Evans archetype with the general formula $[H_y(XO_6)M_6O_{18}]^{n-}$, where y = 0-6, n = 2-8, M = addenda atoms (Mo^{VI} or W^{VI}) and X = a central heteroatom. The Anderson-Evans archetype is a highly flexible POM cluster that allows modification from several point-of-views; i) it can incorporate a large number of different heteroatoms differing in size and oxidation state, ii) it can incorporate inorganic and organic cations and molecules demonstrating different coordination motifs, and iii) covalent attachment with tris(hydroxymethyl)methane ligands allows it to be combined with specific organic functionalities. The catalog of available heteroatoms, counter cations and organic ligands has witnessed a tremendous expansion during the last years ranging from small inorganic anions that act as building-blocks for larger structures to anions in the nanometer range exhibiting multifunctional properties. This in-depth review discusses synthesis approaches and looks into existing Anderson-Evans structures with a special emphasis on structure-property relationship that tris(hydroxymethyl)methane functionalized structures bring. It also covers the successful use of the Anderson-Evans archetype in various fields of classical applications and describes its superiority to other POM archetypes especially in biological applications.

Highlights

- Summary of known inorganic and hybrid Anderson-Evans polyoxometalates.
- Current trends in the synthesis of Anderson-Evans polyoxometalates.
- Challenge: incorporation of multifunctional hybrids into versatile applications.
- Unique advantages of Anderson-Evans clusters compared to other polyoxometalates.

Contents

1. Introduction

Polyoxometalates (POMs) consist of a large class of polynuclear oxo-bridged early transition metal compounds with a rich topology and versatile chemical and physical properties [1]. They are based on the assemblage of MO_n (M = addenda atoms *e.g.* W^{VI}, Mo^{VI}, V^{V}) polyhedra, most commonly octahedra, connected to each other *via* corner and edge sharing. A broad classification splits the POMs into isopolyanions ($[H_xM_yO_z]^{n-}$) and heteropolyanions ($[X_xM_mO_y]^{q-}$, X = heteroatom, *e.g*. a first-row transition metal). The isopolyanions lack heteroatoms resulting in an increased instability compared to heteropolyanions. The metal-oxide framework in heteropolyanions contains a templating heteroatom/heteropolyanion and has been in focus due to the great structural diversity that they bring, including the Keggin $[XM_{12}O_{40}]^{n-}$ [2], Dawson $[XM_{18}O_{62}]^{n-}$ [3] and Anderson-Evans archetypes $[XM_6O_{24}]^{n-}$ [4, 5]. The possibility to attach organic ligands [6] further contributes to the diversity of POM structures allowing the combination of inorganic POMs with specific organic functionalities and thus giving rise to new hybrid compounds [7]. Depending on the i) size, ii) structure, iii) charge, iv) redox chemistry, v) thermal and oxidative stability and vi) photochemistry POMs have become attractive candidates in catalysis [8-11], for sensors [12], in bio− and nanotechnology [13-16], medicine [17-20], material sciences [21], magnetism [22] and macromolecular crystallography [23-31].

Many reviews about POMs have been published addressing *e.g*. different synthetic approaches [32], properties [33-35] and applications [36] in catalysis [37] and biology [17, 31]. Lorenzo-Louis et al. [38] have published a review based on the Anderson-Evans cluster. Since then a lot of work has been reported on this POM archetype. The aim within this review is to give an overview of the Anderson-Evans POM in terms of synthesis and existing structures as well as to demonstrate their suitability for current and new fields of applications. Various different classical uses such as magnetism and catalysis are looked into as well as new research areas in biology since it is becoming one of the go to POMs for biological applications based on recent results in nanomaterials, macromolecular crystallography, tumor inhibiting and antiviral studies. The crystal structures reported herein are based on entries in the Inorganic Crystal Structure Database (www.fiz-karlsruhe.de/icsd.html) and the Cambridge Crystallographic Data Centre (www.ccdc.cam.ac.uk*)*.

2. The Anderson-Evans POM

2.1 The inorganic structure

The Anderson-Evans polyoxoanion is composed of six edge-sharing MoO_6 or WO_6 octahedra surrounding a central, edge-sharing heteroatom of octahedral geometry (XO_6) leading to a planar arrangement and an approximate D_{3d} symmetry [5]. Three different coordination modes of oxygen atoms are found in the structure; six triple-bridged oxygen atoms (μ_3-O) connect the heteroatom and two addenda atoms, six double-bridged oxygen atoms (μ_2-O) connect two addenda atoms and two terminal oxygen atoms (O_t) are connected to each of the six addenda atoms (topview, **Figure 1A**). The general formula can be written as $[H_y(XO_6)M_6O_{18}]^{n-}$, where y = 0-6, n = 2-8, M = addenda atoms (Mo^{VI} or W^{VI}) and X = central heteroatom [1, 38, 39]. A first classification [1] divides the Anderson-Evans structure into two types: the non−protonated A−type with central heteroatoms in high oxidation states with the general formula $[X^{n+}M_6O_{24}]^{(12-n)-}$ (X = *e.g*. Te^{VI} [40], I^{VII} [41]) and the protonated B−type with heteroatoms in low oxidation states and the general formula $[X^{n+}(OH)_6M_6O_{18}]^{(6-n)-}$ (X = *e.g*. Cr^{III} [42], Fe^{III} [43]). The six protons in the B-type are found on the six μ_3-O atoms surrounding the heteroatom [1]. The average dimensions of the Anderson-Evans anion measures approximately 8.6 × 8.6 × 2.7 Å (**Figure 1B**). An isomer of this structure is heptamolybdate ($[Mo_7O_{24}]^{6-}$) [44] representing the "bent" structure (**Figure 1C**). Heptamolybdate can be seen as three edge-shared octahedra in line with two octahedrons located on each side of the space formed in between the three octahedrons. The two octahedrons on each side are shifted by a half octahedron resulting in a "bent" structure (**Figure 1C** bottom). Anderson-Evans-like structures have also been reported with the octahedral heteroatom being replaced by trigonal pyramidal/tetrahedral atoms (*e.g.* V^{V} [45, 46], As^{V} [47] and Te^{IV} [48, 49]) on each side of the planar structure keeping the hexameric addenda ring intact. For color coding of the Figures throughout this review, green/cyan octahedra are used to illustrate addenda atoms that represent either Mo^{VI} or W^{VI} whereas red octahedra represent Mo^{VI} addenda octahedra. Central heteroatoms are given a new color whenever a new XM_6 system is discussed.

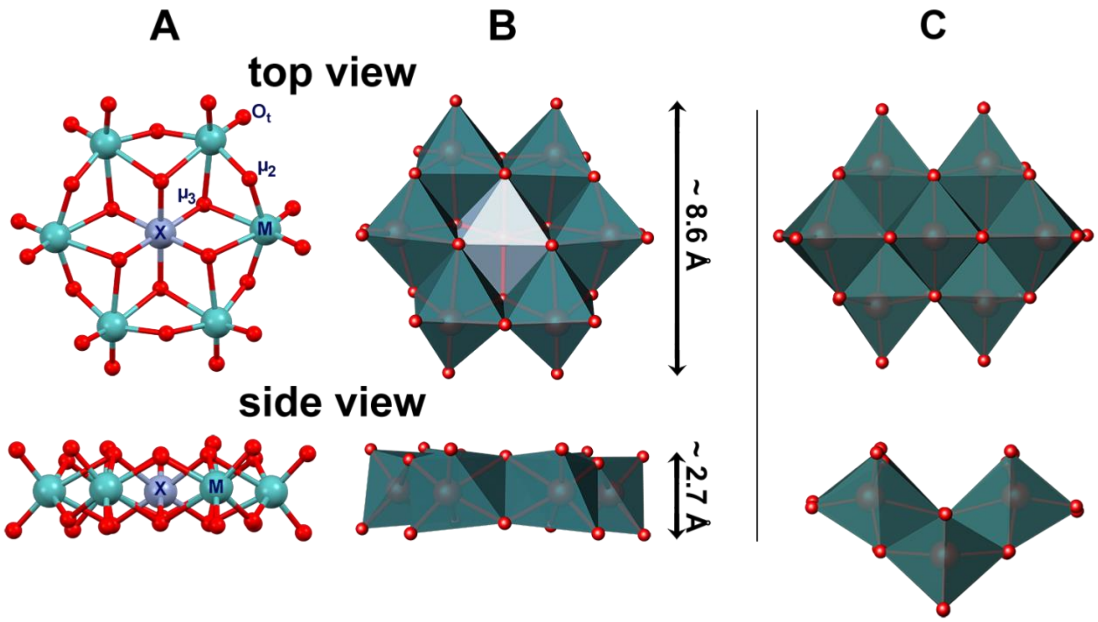

Figure 1. Ball-and-stick (**A**) and polyhedral representation (**B**) of the Anderson-Evans POM $[XM_6O_{24}]^{n-}$ seen from a top view and a side view consisting of the heteroatom (grey sphere, grey octahedron, X = *e.g.* a first-row transition metal), the addenda atoms (green spheres, green octahedrons, M = W^{VI} or Mo^{VI}) and the three different types of oxygen atoms (red spheres) that make up the structure; triple-bridged (μ_3), double-bridged (μ_2) and terminal oxygen atoms (O_t). The "bent" isomer $[M_7O_{24}]^{n-}$ (**C**) [44].

Figure 2 illustrates the elements found in inorganic Anderson-Evans crystal structures varying in oxidation states from II to VII. The XMo_6 (element symbol red in **Figure 2**) system incorporates a greater variety of heteroatoms than the XW_6 system (element symbol green in **Figure 2**). All first-row transition metals except for Sc and Ti have been reported in the literature (**Table 1**) to act as a heteroatom in the XMo_6 system. The XW_6 system exist with $Mn^{II/IV}$ [50] and Ni^{II} [51-54] forming the B-type Anderson-Evans POM, incorporating six hydrogen atoms which is rather unusual when W act as addenda atoms. Interestingly, given the large number of hybrid structures in the $Mn^{III}Mo_6$ system (**section 5.2**), no inorganic crystal structure exist although synthesis and spectroscopic characterization has been reported [55]. Out of the heavier transitions metals only noble metals have entered so far in both the XMo_6 and XW_6 systems (see **Figure 2**). Post-transition metals and metalloids are also represented with

Al^{III}, Ga^{III}, Sb^{V}, Te^{VI} and I^{VII} in the XMo_6 system and Sb^{V} and Te^{VI} in the XW_6 system, however, both systems are still missing several heteroatoms that in theory are accessible based on the ionic radius of the heteroatom. Noble metals such as $Ru^{II/III}$ and Rh^{II} are not represented in either system and several of the first-row transition metals are missing in the XW_6 system like Cr, Fe, Co and Cu. Inorganic counter cations (element symbol orange in **Figure 2**) have instead been widely explored. This includes the majority of the alkali metals and alkaline earth metals as well as the entire lanthanide series.

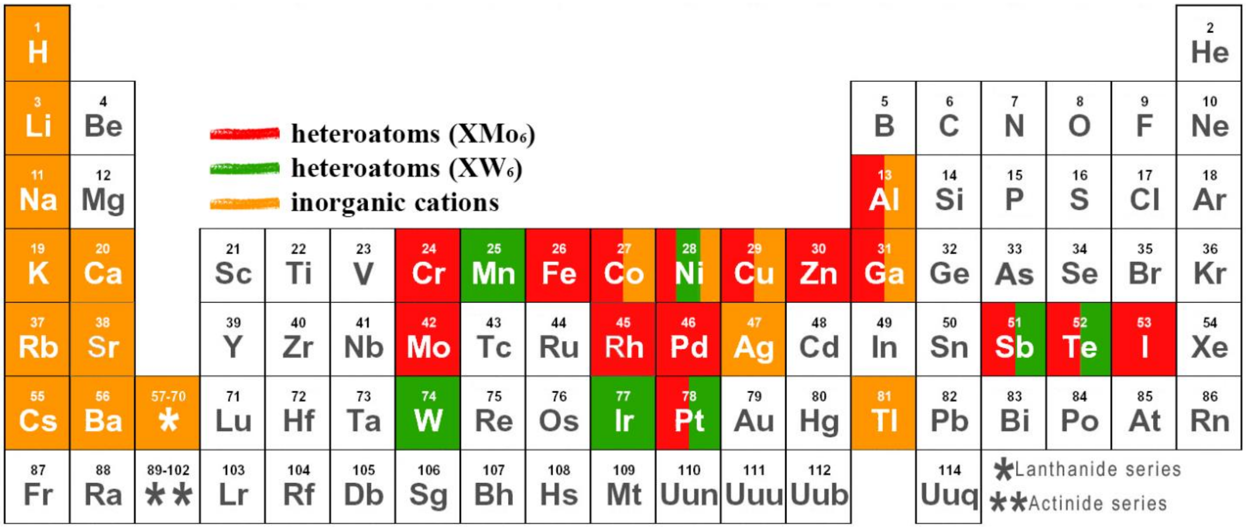

Figure 2. Periodic table illustrating heteroatoms in XMo_6 and XW_6 systems and the different cation linkers successfully applied.

The Anderson-Evans structure exhibits physical and chemical properties that are highly versatile but depend strongly on the heteroatom, counter cation and any organic functionalization (see chapter 2.2). One property that arise from the specific geometry of the POM and/or the addenda atoms making it applicable for the majority of the compounds are $p_{\pi}(O_t) \rightarrow d_{\pi*}(Mo)$ ligand-to-metal charge-transfer transitions that are characteristic for the Anderson-Evans-type framework. They appear at approximately 210 nm with a shoulder at 240 nm [56-61] and can be characterized by more absorption bands [62] depending on the presence of any further absorbing elements/units. The Anderson-Evans POM is hydrolytically stable enabling its application in biology. There are only a few papers discussing the hydrolytic stability of the Anderson-Evans POM in the $GaMo_6$ [57], $CrMo_6$ [63] and the Anderson-Evans like VMo_6 system [64]. The thermal stability has also been thoroughly investigated in several different systems [57, 60, 61, 65-70] and the above mentioned factors can have significant impact on the thermal stability. The redox properties strongly depend on the heteroatom and pH and have been investigated in the $CoMo_6$ [71], IrW_6 [72], $CrMo_6$ [73], $AlMo_6$ [74], $TeMo_6$ [70] and TeW_6 [75] systems. The magnetic behavior in Anderson-Evans POMs depends on the heteroatom present, symmetry and the presence of any well-defined ligands with polynuclear transition metal clusters and is discussed in **section 6.4**. Several Anderson-Evans POMs exhibit luminescent emission bands which have been reported in the $AlMo_6$ [76-78], $CrMo_6$ [58, 67, 76, 79] and SbW_6 [80] systems. The luminescent properties strongly depend on the incorporation of any luminescent atoms and symmetry (**section 3**).

2.2 Topology of “extended“ organic-inorganic and tris-functionalized hybrid structures

Compounds containing organic molecules that are non-covalently attached to the POM have resulted in a variety of “extended” structures with subsequent solid-state applications (see **sections 6.4-6.5**). Covalent attachment has, except in [81, 82] (see **section 5.2**), been grafted with a variety of organic tris(hydroxymethyl)methane ligands ($RC(CH_2OH)_3$), abbreviated with “tris” in this review. The organic ligands are usually connected to the POM *via* terminal oxygen atoms (O_t) (**Figure 1A**) in “extended” structures, whereas the covalent attachment to the POM has, except in [81, 82], been functionalized with tris-ligands at μ_2-O and μ_3-O atoms (**Figure 3**).

The general build-up of the “extended” structures consist of metals like Cu, that act as linkage between organic ligands like pyridine-4-carboxylic acid that offers nitrogen and oxygen donor atoms and the Anderson-Evans POM providing oxygen donor atoms. This sort of template building, where the POM clusters act as building units to form a high-dimensional solid-state material is reported in B-type systems but has also been widely reported in A-type systems with heteroatoms such as Te^{VI} and I^{VII} since they lack six proton ligands (μ_3-OH, see **Figure 1A**) that can be replaced with tris-ligands.

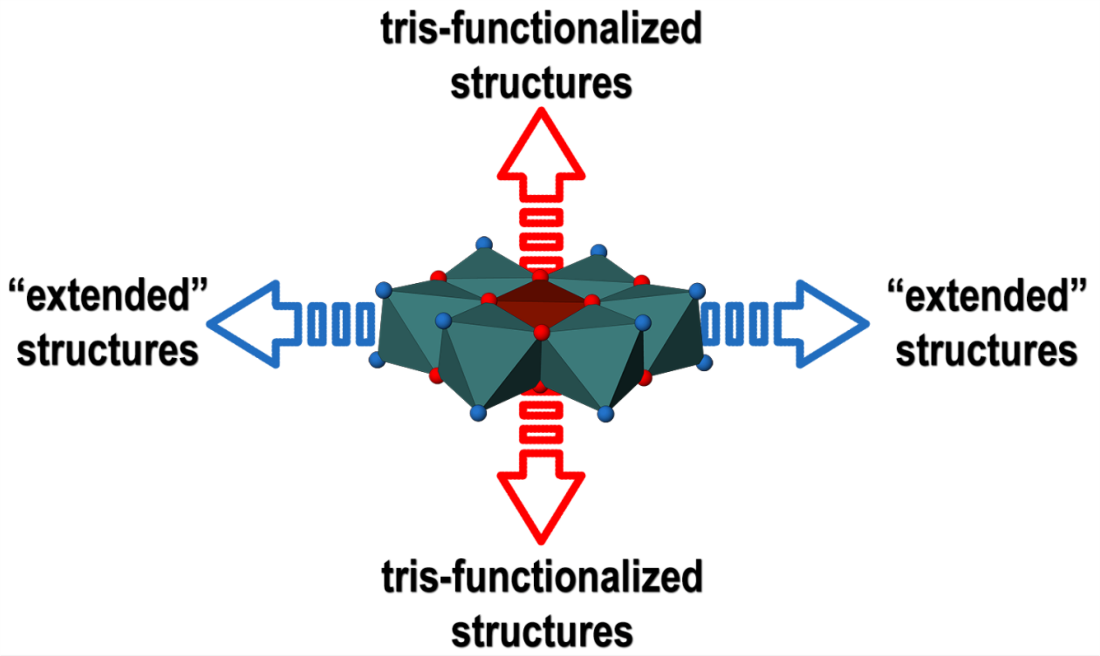

Figure 3. Schematic illustration of where the majority of the reported “extended” and covalently attached hybrid structures connect to the Anderson-Evans POM framework. The “extended” structures usually connect with the cluster on terminal oxygen atoms O_t (blue spheres) whereas covalently attached tris-ligands are grafted on the planar POM surface at μ_2-O and μ_3-O atoms (red spheres). Green octahedra: addenda atoms (Mo^{VI} for tris-functionalized structures and Mo^{VI}/W^{VI} for “extended” structures); dark red octahedron: central heteroatom.

The six protons attached to μ_3-O atoms (**Figure 1A**) of the Anderson-Evans POM in the B−type can be replaced with a wide variety of tris-ligands ($RC(CH_2OH)_3$, R = *e.g.* $-NH_2$, -OH, $-CH_2OH$, and further derivatization with imine and amide bonds either before or after attachment to the POM) [83, 84]. The tris-ligands can be synthesized first and then be grafted onto the POM (*pre*-functionalization) or tris-ligands can further be modified by organic reactions after attachment onto the POM (*post*-functionalization) [85]. They may cap either a tetrahedral cavity by connecting to two μ_3-O atoms and one μ_2-O atom (χ-isomer, **Figure 4A**) or by capping the templating heteroatom and connecting to three μ_3-O atoms (δ-isomer, **Figure 4B**) [86]. Due to the rather high symmetry of the inorganic Anderson-Evans POM and the presence of protonated μ_3-O atoms on both sides of the planar structure, functionalization with tris-ligands naturally results in double-sided products (**Figure 4C**) but both isomers can be synthesized single-sided (**Figure 4A-B**) too (see **section 4.2.2**).

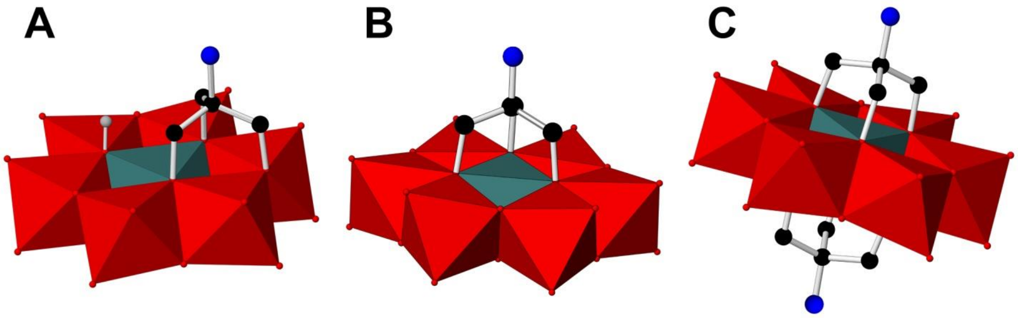

Figure 4. Combined ball-and-stick and polyhedral representation of single-sided χ-isomer (**A**), single-sided δ-isomer (**B**) and double-sided δ-isomer (**C**). Red octahedra: Mo; green octahedra: heteroatom in a low oxidation state; black spheres: C; blue spheres: N; red spheres: O; grey sphere: H.

Figure 5 shows the periodic table and highlights heteroatoms that have been functionalized with tris-ligands [86]. All known tris-functionalized systems are in the XMo_6 system with the majority of the reported structures containing Mn^{III} or Cr^{III} heteroatoms. Compared to the pure inorganic structures (**Figure 2**), this field is rather unexplored in terms of heteroatoms but the variety in ligands attached onto *e.g.* $Cr^{III}Mo_6$ and $Mn^{III}Mo_6$ has seen far more variety and is still increasing in a fast paste (**Table 2, Section 5.2**). Besides the apparent lack of tris-functionalized XW_6 systems, several other heteroatoms are still missing in the XMo_6 system with a tris-functionalization which should be accessible [1], like Co, Cu, Pt, and Te.

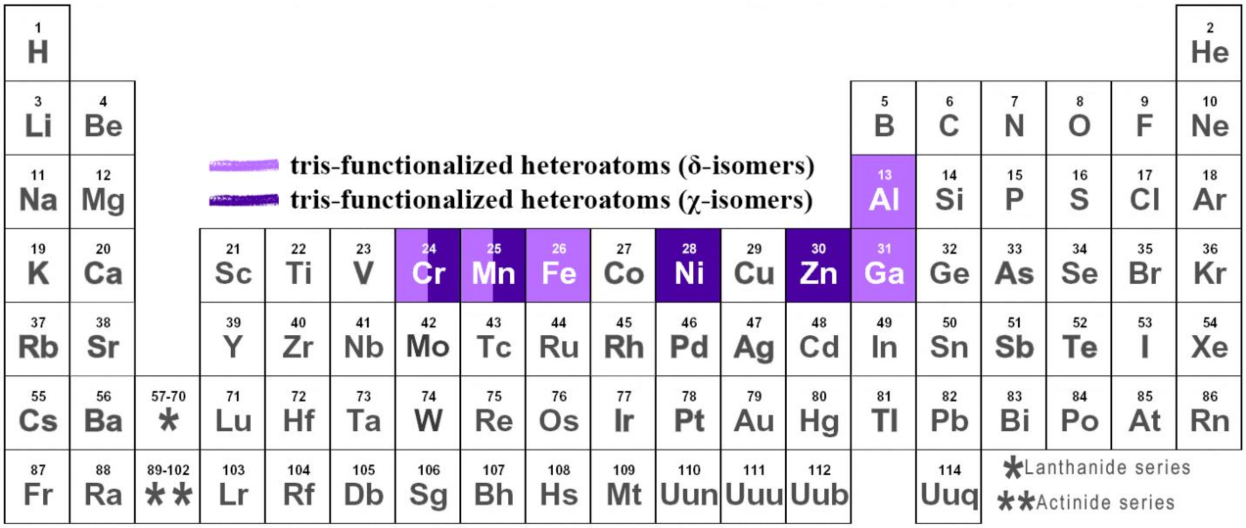

Figure 5. Periodic table illustrating heteroatoms in the XMo_6 system containing tris-functionalized structures either as the δ or as the χ-isomer.

3. Inorganic Anderson-Evans POMs: The great variety of heteroatoms

In 1937 Anderson proposed the A-type structure $[Te^{VI}Mo_6O_{24}]^{6-}$ [4, 87], and was later confirmed with X-ray diffraction experiments in 1948 by Evans [5]. The six protons in the B-type Anderson-Evans POM were first reported in $Na_3[Cr(OH)_6Mo_6O_{18}] \times 8H_2O$ from the known valence states of the atoms in the anion and the net charge [42]. Since these milestone findings many new inorganic crystal structures of Anderson-Evans POMs have been reported which are summarized in **Table 1**.

Table 1. The inorganic crystal structures containing the Anderson-Evans structure in the XMo_6 (left column) and XW_6 (right column) systems. For each XM_6 system (X = heteroatom, M = addenda atom), the ionic radius of the heteroatom and the average heteroatom – oxygen atom (μ_3-O) distance is given. The average distance is based on all six X-(μ_3-O) distances from all crystal structures within the same XM_6 system. The structures are arranged in an increasing atomic number of the templating heteroatom and under each XM_6 system the structures are given low oxidation state to high. Within the same oxidation state the compounds are given in a chronological order with the oldest crystal structures reported first.

XMo_6			**XW_6**		
Compound	**Ionic radius of X (pm)**	**Avg. X-(μ_3-O) dist.**	**Compound**	**Ionic radius of X (pm)**	**Avg. X-(μ_3-O) dist.**
$Al^{III}Mo_6$	**67.5**	**1.89**	**no equivalent**		
$K_3H_6[AlMo_6(OH)_6O_{18}]$ x $7H_2O$ [88]					
$[Ln(H_2O)_7][Al(OH)_6Mo_6O_{18}]_n$ x $4nH_2O$ [89]					
$Na_{3n}(H_2O)_{6n}[Al(OH)_6Mo_6O_{18}]_n$ x $2nH_2O$ [90]					
$(NH_4)_3[AlMo_6O_{24}H_6]$ [91]					
$Na_3(H_2O)_6[Al(OH)_6Mo_6O_{18}]$ x $2H_2O$ [92]					
$H_3[AlMo_6(OH)_6O_{18}]$ x $10H_2O$ [93]					
$Na_2(H_2O)_4(H_3O)[Al(OH)_6Mo_6O_{18}]$ [94]					
$[Eu(H_2O)_7][Al(OH)_6Mo_6O_{18}]$ x $4H_2O$ [78]					
$[Al(H_2O)_6][Al(OH)_6Mo_6O_{18}]$ x $10H_2O$ [95]					
$Cr^{III}Mo_6$	**75.5**	**1.97**	**no equivalent**		

$Na_3[Cr(OH)_6Mo_6O_{18}]$ x $8H_2O$ [42] $Ga[CrMo_6O_{18}(OH)_6]$ x $16H_2O$ [96] $[(H_2O)_4Ag_3][Cr(OH)_6Mo_6O_{18}]$ x $3H_2O$ [97] $[Na_3(H_2O)_{11}][CrMo_6O_{24}H_6]$ x $2H_2O$ [98] $[NdCrMo_6O_{18}(OH)_6(H_2O)_7]$ x $4H_2O$ [99] $[X^{III}(H_2O)_7Cr(OH)_6Mo_6O_{18}]_n$ x $4nH_2O$ (X = Ce, Sm, Eu) [58] $[Tm_2(H_2O)_{14}CrMo_6O_{24}H_6][CrMo_6O_{24}H_6]$ x $16H_2O$ [100] $[Pr(H_2O)_7][CrMo_6H_6O_{24}]$ x $4H_2O$ [59] $[Al(H_2O)_6][Cr(OH)_6Mo_6O_{18}]$ x $10H_2O$ [101] $[NH_4]_3[CrMo_6O_{18}(OH)_6]$ [102] $K_2[H_7CrMo_6O_{24}]$ x $8H_2O$ [103] [104]					
$Fe^{II}Mo_6$ $[Na_4(H_2O)_7][Fe(OH)_6Mo_6O_{18}]$ [43]	**78.5**	**2.01**	**no equivalent**		
no equivalent			**$Mn^{IV}W_6$** $Na_8[MnW_6O_{24}]$ × $18H_2O$ [105] $K_6Na_2[MnW_6O_{24}]$ × $12H_2O$ [106]	**67**	**1.92**
no equivalent			**$Mn^{II}W_6$** $[Na_2(H_2O)_{10}][Na(H_2O)_3]_2[MnW_6O_{18}(OH)_6]$ × $6H_2O$ [50]	**81**	**1.91**
$Co^{III}Mo_6$ $[Ga(H_2O)_6][Co(OH)_6Mo_6O_{18}]$ × $8H_2O$ [107] $Ba_3[Co(OH)_6Mo_6O_{18}]_2$× $20H_2O$ [108] $Na_3[H_6CoMo_6O_{24}]$ × $8H_2O$ [71] $K_3[H_6CoMo_6O_{24}]$ × KNO_3 × $4H_2O$ [109] $K_3[H_6CoMo_6O_{24}]$ × $7H_2O$ [110] $Ga[CoMo_6O_{18}(OH)_6]$× $16H_2O$ [111] $(NH_4)_3[CoMo_6O_{24}H_6]$ [91] $[Cu(NH_3)_4]H[CoMo_6O_{18}(OH)_6]$ × $10H_2O$ [112] $(NH_4)_4[H_6CoMo_6O_{24}]$ × $4H_2O$ [113]	**75**	**1.91**	**no equivalent**		
$Ni^{II}Mo_6$ $[\{Ni(H_2O)_4\}_2\{Ni(OH)_6Mo_6O_{18}\}]$ × $4H_2O$ [114] $(NH_4)_4[H_6NiMo_6O_{24}]$ × $4H_2O$ [115] $(NH_4)_2[Na_2Ni(OH)_6Mo_6O_{18}(H_2O)_2]$ [116] $[Ni(H_2O)_6][Ag_2\{Ni(OH)_6Mo_6O_{18}\}]$ × $8H_2O$ [114]	**83**	**2.04**	**$Ni^{II}W_6$** $X_4[NiW_6O_{24}H_6]$ × nH_2O (X = K, Rb, Cs, Tl, Ni) [53] $X_2[NiW_6O_{24}H_6]$ × nH_2O (X = Ca, Sr, Ba) [54] $Na_4[NiW_6O_{24}H_6]$ × $13H_2O$ [52] $Na_4[Ni(OH)_6W_6O_{18}]$ × $16H_2O$ [51]	**83**	**2.04**
$Cu^{II}Mo_6$ $(NH_4)_4[H_6CuMo_6O_{24}]$ × $4H_2O$ [117]	**87**	**2.06**	**no equivalent**		
$Zn^{II}Mo_6$ $(NH_4)_4(H_6ZnMo_6O_{24})$ × $6H_2O$ [118]	**88**	**2.08**	**no equivalent**		
$Ga^{III}Mo_6$ $X_3[GaMo_6(OH)_6O_{18}]$ × $7H_2O$ (X = NH_4 [119], K [120])	**76**	**1.97**	**no equivalent**		
Mo^{VI}_7* $(NH_4)_6[Mo_7O_{24}]$ × $4H_2O$ [44, 121, 122] $X_6[Mo_7O_{24}]$ × nH_2O (X = K; n = 4 [121] X = Cs; n = 7 [123]) $NaCs_5[Mo_7O_{24}]$ × $5H_2O$ [124] $Na_7[Mo_7O_{24}]OH$ × $21H_2O$ [125] $K_6[Mo_7O_{22}(O_2)_2]$ × $9H_2O$ [126] $Na_6(Mo_7O_{24})$ × $14H_2O$ [127]	**73**	**1.97**	**no equivalent**		
$Rh^{III}Mo_6$ $(NH_4)_3[H_6RhMo_6O_{24}]$ × $6H_2O$ [128]	**80.5**	**2.02**	**no equivalent**		

$Ga[RhMo_6O_{18}(OH)_6] \times 16H_2O$ [129]					
$Pd^{IV}Mo_6$	**75.5**	**1.99**	**no equivalent**		
$K_{0.75}Na_{3.75}[PdMo_6O_{24}H_{3.5}] \times 17H_2O$ [130]					
$Sb^{V}Mo_6$	**74**	**1.98**	**$Sb^{V}W_6$**	**74**	**1.99**
$K_5[H_2SbMo_6O_{24}] \times 7H_2O$ [131]			$K_5Na_2[SbW_6O_{24}] \times 12H_2O$ [132] $K_{5.5}H_{1.5}[SbW_6O_{24}] \times 6H_2O$ [80]		
$Te^{VI}Mo_6$	**70**	**1.93**	**$Te^{VI}W_6$**	**70**	**1.93**
$(NH_4)_6[TeMo_6O_{24}] \times 7H_2O$ (X = (NH4) [5, 87], K [5]; n = 7) $X_6[TeMo_6O_{24}] \times yTe(OH)_6 \times nH_2O$ (X = (NH4); y = 1; n = 7 [87] X = Rb; y = 1 n = 6 [133] X = Li; y = 1 n = 18 [134] X = Cs; y = 2; n= 4 [135]) $X[TeMo_6O_{24}] \times nH_2O$ (X = Rb_6; n = 10 [133] X = Li_6; n = 18 [134] X = Na_6; n = 22 [137] X = $Na_4(NH_4)_2$; n = 16 [138]) $[X(H_2O)_6]_3[TeMo_6O_{24}]$ (X = Co, Ni) [139] $\{[La(H_2O)_6]_2[TeMo_6O_{24}]\}_n \times 6nH_2O$ [140] $\{[Ce(H_2O)_7]_2[TeMo_6O_{24}]\}_n \times 7nH_2O$ [140] $\{[X(H_2O)_7]_2[TeMo_6O_{24}]\}_n \times 8nH_2O$ (X = Pr, Nd) [140] $K_{6n}(TeMo_6O_{24})_n[(X(H_2O)_7)_2(TeMo_6O_{24})]_n \times 16nH_2O$ (X = Eu, Gd) [141] $K_{3n}[X(H_2O)_5(TeMo_6O_{24})]_n \times 6nH_2O$ (X = Tb, Dy, Ho, Er) [141] $[(X(H_2O)_6)_2(TeMo_6O_{24})] \times 10H_2O$ (X = Ho, Yb) [142] $Nd_2[TeMo_6O_{24}] \times 18H_2O$ (n = 18 [143] n = 19 [144]) $(NH_4)_2\{[X(H_2O)_3]_2[TeMo_6O_{24}]\} \times H_2O$ (X = Mn, Co, Ni, Cu, Zn) [145] $[X(H_2O)_4]_2[TeMo_6O_{24}] \times 3H_2O$ (X = La, Ce, Nd) [145] $[X(H_2O)_7]_2[TeMo_6O_{24}] \times 6H_2O$ (X = La, Ce, Pr, Sm) [146] $\{[Sm(H_2O)_5]_2(TeMo_6O_{24})\} \times 6H_2O$ [147] $\{[Eu(H_2O)_7]_2(TeMo_6O_{24})\} \times 5H_2O$ [147]			$Na_6[TeW_6O_{24}] \times 22H_2O$ [40] $(NH_4)_2\{[Ni(H_2O)_3]_2[TeW_6O_{24}]\} \times H_2O$ [136]		
$I^{VII}Mo_6$	**67**	**1.88**	**no equivalent**		
$K_5[IMo_6O_{24}]_2 \times 5H_2O$ [41] $[Cr(H_2O)_6][Na_2(H2O)_{10}][IMo_6O_{24}] \times 8H_2O$ [148] $Na_4[Pr(H_2O)_5]_2[IMo_6O_{24}]_2 \times 7H_2O$ [149]					
no equivalent			**W^{VI}_7***	**74**	**2.01**
			$Na_6[W_7O_{24}] \times 14H_2O$ [150] [151]		
no equivalent			**$Ir^{IV}W_6$**	**76.5**	**2.00**
			$Na_6H[HIrW_6O_{24}] \times 26H_2O$ [72]		
$Pt^{IV}Mo_6$	**76.5**	**2.00**	**$Pt^{IV}W_6$**	**76.5**	**2.01**
$K_4[H_4\beta\text{-}PtMo_6O_{24}] \times 2H_2O$ [152] $(NH_4)_{4.5}H_{3.5}[\alpha PtMo_6O_{24}] \times 1.5H_2O$ [154] $K_{3.5}[\alpha\text{-}H_{4.5}PtMo_6O_{24}] \times 3H_2O$ [152, 156] $K_2[H_6\alpha PtMo_6O_{24}] \times 5H_2O$ (n = 5 [158] 6 [159]) $X_2[H_2\alpha\text{-}PtMo_6O_{24}] \times nH_2O$ (X = Nd; n = 14 [161] X = La; n = 16 [162]) $K_{3.5}[H_{4.5}\alpha PtMo_6O_{24}] \times 5.5H_2O$ [164] $KNa[H_6\alpha\text{-}PtMo_6O_{24}] \times 6H_2O$ (n = 6 [166] 11 [167]) $K_7[H_9\alpha\text{-}Pt_2Mo_{12}O_{48}] \times 11H_2O$ [169]			$Na_5[H_3PtW_6O_{24}] \times 20H_2O$ [153] $K_6Na_2[PtW_6O_{24}] \times 12H_2O$ [155] $K_{2.5}[H_{5.5}PtW_6O_{24}] \times 2H_2O$ [157] $K_5[H_3PtW_6O_{24}] \times 6H_2O$ [160] $Na_8[PtW_6O_{24}] \times 26H_2O$ [163] $Na_6[H_2PtW_6O_{24}] \times 22H_2O$ [165] $Na_{5.5}[H_{2.5}PtW_6O_{24}] \times 17H_2O$ [168]		
$Pt^{IV}Mo_6$*	**76.5**	**2.00**	**no equivalent**		
$(NH_4)_4[\beta\text{-}H_4PtMo_6O_{24}] \times 1.5H_2O$ (X = NH_4, K; n = 1.5, 2) [152]					

* Contains the "bent" isomer

X-ray diffraction experiments from the crystal structures in **Table 1** reveal a slightly flattened central octahedron and six surrounding addenda octahedra that form a planar array of distorted octahedra for the Anderson-Evans archetype. The distortion of the Mo/WO$_6$ units derives from the outwards expansion of the addenda atoms, which is characteristic for the Anderson-Evans structure. The M-O bond distances and angels are all influenced by the heteroatom. Larger heteroatoms give longer X-(μ_3-O) bonds and subsequently longer M-O bond distances and increased M-O-M angles whereas the reverse is observed for smaller heteroatoms. The M-(μ-O) bond distance increases when the central heteroatom binds stronger, as seen for example in Mn^{IV}W$_6$ structures. The ionic radius of heteroatoms varies between 67 and 88 pm in XMo$_6$ systems and 67 to 83 pm in XW$_6$ systems. It is directly related to the average bond-distances observed around the six μ_3-O atoms surrounding the heteroatom. The variance in the average X-(μ_3-O) bond distance among the different heteroatoms spans 0.2 Å (from 1.88 to 2.08 Å) for the heteroatoms in both the XMo$_6$ and XW$_6$ systems. The shortest average distance of 1.88 Å is in the I^{VII}Mo$_6$ (67 pm) system containing the smallest heteroatom, whereas the longest average distance is in the Zn^{II}Mo$_6$ (88 pm) structures containing the largest heteroatom. Thus, the hexameric addenda ring shows great flexibility towards outwards/inwards expansion to accommodate for a wide range of heteroatoms.

The structures in **Table 1** show great variety of counter cations. Monovalent, divalent and trivalent cations have been observed and sometimes the same species [95, 114] acts as both the heteroatom and counter cation. Depending on the valence of the anions and cations the Anderson-Evans anion can act as a monodentate, bidentate or multidentate ligand [59, 97]. The size of the cation can also determine the coordination mode to the POM. When trivalent rare earth cations were used with [TeMo$_6$O$_{24}$]$^{6-}$ the anion acted as either a hexadentate ligand for smaller cations (La^{III}) or as a tetradentate ligand for larger cations (Ce^{III}, Pr^{III}, Nd^{III}) [140]. Different modes of linkage have also been observed, as in the case with [Na$_3$(H$_2$O)$_{11}$][CrMo$_6$O$_{24}$H$_6$] × 2H$_2$O, containing the cation [Na$_3$(H$_2$O)$_{11}$]$^{3+}$, where the cation forms a chain increasing the distance between the anions (**Figure 6**) [98]. The specific coordination of the cations can have remarkable effects on physical properties of the entire complex. In the complex [Tm$_2$(H$_2$O)$_{14}$CrMo$_6$O$_{24}$H$_6$][CrMo$_6$O$_{24}$H$_6$] × 16H$_2$O the cations may be responsible for specific single-crystal-to-single-crystal phase transition [100].

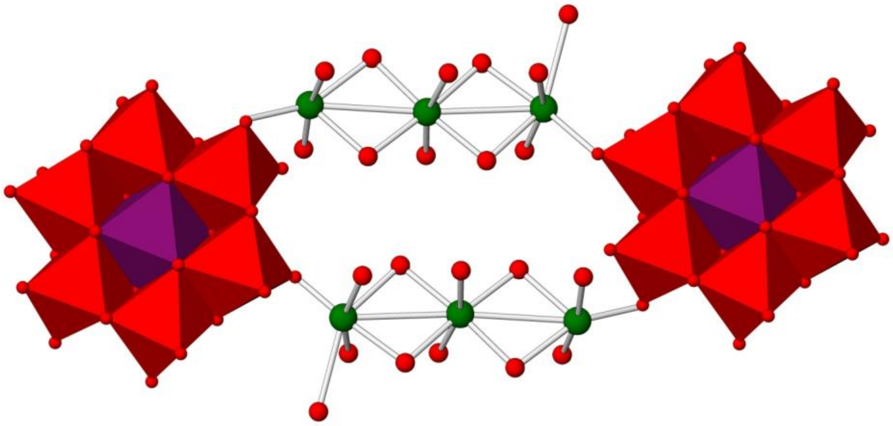

Figure 6. Ball-and-stick representation of $\{[Na_3(H_2O)_{11}][CrMo_6O_{24}H_6]\}_2$ showing an increased distance between the $[CrMo_6O_{24}H_6]^{3-}$ anions. Red octahedra: Mo; purple octahedra: Cr; green spheres: Na; red spheres: O.

The compound $[Eu(H_2O)_7][Al(OH)_6Mo_6O_{18}] \times 4H_2O$ incorporates Eu and exhibits photoluminescence with an emission maximum at 591 nm corresponding to the $^5D_0 \rightarrow {}^7F_1$ transition. However, when glycine is introduced, as in $\{(C_2H_5NO_2)_2[Eu(H_2O)_5]\}[Al(OH)_6Mo_6O_{18}] \times 10H_2O$ ($C_2H_5NO_2$ = glycine), a different crystal packing is induced that increases the symmetry and thus significantly increases the intensity of the $^5D_0 \rightarrow {}^7F_1$ transition compared to the compound that lacks the glycine molecules. Thus, the photoluminescence is enhanced but the opposite can also occur and certain emission bands can disappear as well from *e.g.* rare-earth ions with well-known emission capabilities, especially the sharp characteristic 4f absorption or emission peak [79].

It is also common for the supramolecular inorganic Anderson-Evans structures in the solid-state to incorporate water molecules which usually act as guests since the majority of the compounds are isolated from aqueous solutions (see **section 4.1**) [92, 170]. In the compound, $[Al(H_2O)_6][Al(OH)_6Mo_6O_{18}] \times 10H_2O$, where Al^{III} is observed to act as both a heteroatom and counter cation, it balanced the charge but also allowed formation of unique water sheets composed of water hexamers in both chair- and boat-form [95].

4. Synthesis of Anderson-Evans POM

4.1 Synthesis of inorganic structures

The general procedure to synthesize inorganic Anderson-Evans POMs is rather straightforward and involves acidifying an aqueous solution containing metal-oxide anions (MoO_4^{2-}, WO_4^{2-}) and a salt of a templating heteroatom. Synthetic variables include (i) the concentration and type of metal-oxide anions; (ii) the pH and type of acid used; (iii) the type and concentration of heteroatom; (iv) the introduction of any additional ligands; (v) the use of reducing agent; (vi) the temperature of the reaction mixture and (vii) the solvent used. There are two common synthesis techniques used to obtain inorganic clusters, the hydrothermal and the aqueous refluxing synthesis. Hydrothermal synthesis allows crystallizing substances from high-temperature aqueous solutions at high vapor pressures, which is becoming more popular [73, 136, 145, 147, 171-177] and controllable but is still rather sensitive towards physical parameters. Thus, the aqueous synthesis under reflux remains the conventional synthesis route for inorganic clusters. The introduction of different counter cations is usually done during the synthesis but sometimes cation exchange of already synthesized Anderson-Evans clusters are necessary to obtain the Anderson-Evans structure with the counter cation of interest [59].

4.2. Synthesis of “extended” organic-inorganic and hybrid tris-functionalized structures

4.2.1 Synthesis of “extended” organic-inorganic structures

For organic-inorganic structures the introduction of the organic ligands in solution is usually enough since covalent bond formation does not take place. However, despite the rather simple synthesis approach, the presented examples in **sections 5** and **6** underline the important effect of the choice of chemicals on the final structure and its properties since it gives access to various topologies.

4.2.2 Synthesis of tris-functionalized hybrid structures

Figure 7 summarizes the different synthesis routes so far explored for tris-functionalized Anderson-Evans POMs as well as the different products possible with each procedure. Several approaches have been applied, (i) re-arrangement of octamolybdate (**Figure 7 A1-A4**), (ii) applying *pre*-synthesized Anderson-Evans POMs in polar solvents (**Figure 7, B1-B5**) and (iii) activation of μ_2-O atoms to form the χ-isomer (**Figure 7, C1-C5**).

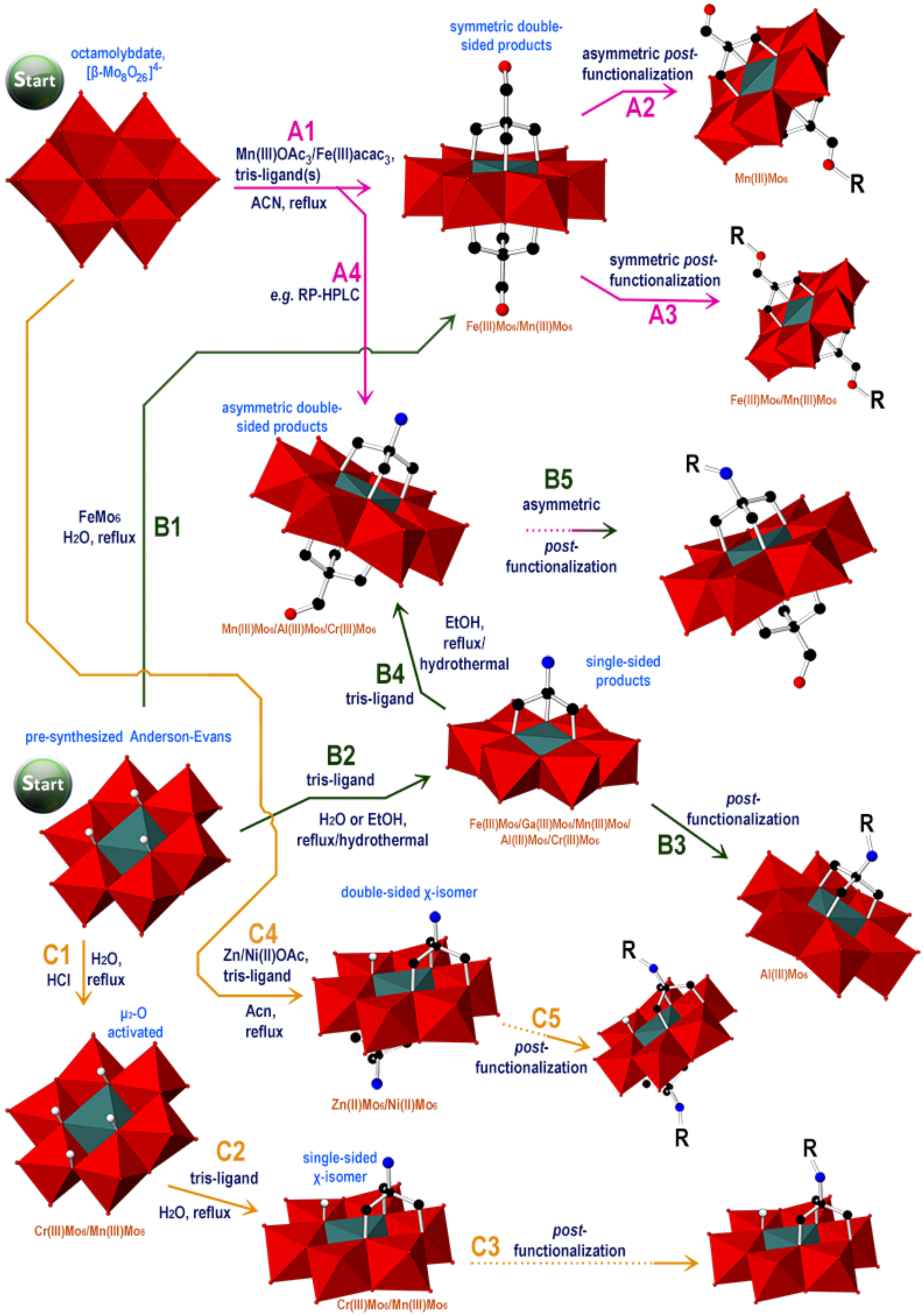

Figure 7. A schematic summary of the different synthesis strategies used in the preparation of tris-functionalized Anderson-Evans POMs. They are synthesized either through re-arrangement of octamolybdate (**A1-A4**, pink) or by using pre-synthesized Anderson-Evans POMs (**B1-B5**, green) which gives the δ-isomer. The χ-isomer can also be obtained (**C1-C5**, orange) both single-sided (**C1-C3**) and double-sided (**C4-C5**). For each step the general synthesis conditions are given as well as heteroatoms that have been reported. Dashed arrows are theoretically accessible functionalization steps that have not been reported yet. Red octahedra: Mo; green octahedra: heteroatom in a low oxidation state; black spheres: C; blue spheres: N; red spheres: O; white spheres: H.

4.2.2.1 Synthesis of tris-functionalized δ-isomers by re-arrangement of octamolybdate

In 2002 Hasenknopf et al. [86] reported on the $[MnMo_6O_{18}\{(OCH_2)_3CNO_2\}_2]^{3-}$ anion, which was the first ever report of a tris-functionalized Anderson-Evans POMs. The compound was obtained by refluxing acetylacetonate or acetate salts of the templating heteroatom (Mn^{III}) together with $[TBA]_4[\alpha\text{-}Mo_8O_{26}]$ and tris-NO_2 in acetonitrile (**Figure 7, A1**). The six protons on the μ_3-O atoms surrounding the Mn^{III} heteroatom on both sides are replaced by the tris-ligands giving the δ-isomer (**Figure 4B**) [86]. Rosnes et al. [178] showed that both isomers $[\alpha\text{-}Mo_8O_{26}]^{4-}$ and $[\beta\text{-}Mo_8O_{26}]^{4-}$ [179, 180] can be used to synthesize hybrid organic-inorganic $Mn^{III}Mo_6$ compounds. The β-isomer is shown in the upper left corner in **Figure 7** and the α-isomer differs by incorporating two tetrahedrons instead of the two central octahedrons on each side. The reaction media can also be exchanged with DMF making it possible to use ligands that are not soluble in acetonitrile and the desired cations may be directly introduced, even small inorganic cations [178]. Since then symmetric *post*-functionalization (**Figure 7, A3**) has been achieved with a variety of organic ligands including ligands containing aromatic units [181] and alkyl-chains [182] of different lengths (see **section 5.2**).

Asymmetric double-sided hybrid organic-inorganic Anderson-Evans POMs have also been obtained [183] *via* the re-arrangement of octamolybdate (**Figure 7, A4**), which was initially achieved with tris-NO_2 decorated on one side and tris-CH_3 on the other [184]. The synthesis involves a reaction mixture containing both tris-ligands, which naturally results in a mixture of three different anions; two symmetrical products (**Figure 7, A1**) of each organic ligand and one asymmetric (**Figure 7, A4**) product. By separating crystals from the mother liquor every six hours and applying ESI-MS the three different products were isolated. More recent methods take advantage of the difference in polarity between the three products and were therefore separated by means of RP-HPLC [85]. If the difference in polarity is too small, protective groups may be used to allow proper separation with the possibility of subsequent *post*-functionalization once isolated [85]. The only report of an asymmetric *post*-functionalization (**Figure 7, A2**) involves the attachment of SP to $[MnMo_6O_{18}\{(OCH_2)_3CNH_2\}_2]^{3-}$. Interestingly, the diffraction experiment revealed attachment of spiropyran on one side only leaving the amino group unreacted on the tris-ligand on the opposite side. The symmetrical product was also obtained but no crystals could be obtained [185]. This finding gives an insight on the reaction mechanism, which suggests that the *post*-functionalization proceeds with attachment of one organic ligand on one side first before the second ligand is attached.

4.2.2.2 Synthesis of tris-functionalized δ-isomers with *pre*-synthesized Anderson-Evans POMs

By applying *pre*-synthesized Anderson-Evans POMs the rather complicated reconstruction process from octamolybdate (**Figure 7, A1**) is avoided giving room for more controllable reaction sites of the organic ligand onto the Anderson-Evans POM [186]. Wu et al. [187] recently reported on the first single-side tris-functionalized Anderson-Evans POM (**Figure 7, B2**) by grafting tris-CH_2-OH onto $[Cr(OH)_6Mo_6O_{18}]^{3-}$. Single-side decoration has since then been reported in the $Fe^{III}Mo_6$, $Al^{III}Mo_6$, $Ga^{III}Mo_6$ and $Mn^{III}Mo_6$ systems (see **Table 2**). The reason for the single-side decoration was argued to be the aqueous reaction media since the single-side decorated product is always obtained, regardless of the POM to organic ligand ratio. However, recent findings on the single-side tris-decoration of $Ga^{III}Mo_6$ and $Fe^{III}Mo_6$ systems with tris-NH_2 and tris-CH_2-OH yielded both single-sided (**Figure 7, B2**) and double-sided (**Figure 7, B1**) products [57]. Thus, tris-ligands and heteroatoms also play important roles in the mechanism of the single-side grafting, besides the already reported [187] aqueous environment. Further *post*-functionalization of single-sided products (**Figure 7, B3**) is a guarantee for keeping the single-side decoration.

The ability to decorate Anderson-Evans POMs in a step-by-step fashion with two different tris-ligands on each side (**Figure 7, B2 and B4**) can be prepared through a hydrothermal procedure by using water as solvent [171] or by refluxing in hot ethanol [188] giving asymmetrical double-sided products. The hydrothermal method was demonstrated with $Cr^{III}Mo_6$ whereas refluxing in hot ethanol was achieved with $Cr^{III}Mo_6$, $Al^{III}Mo_6$ and $Mn^{III}Mo_6$ systems (**Figure 7, B2 and B4**) in a step-by-step fashion by refluxing. Interestingly, the use of ethanol also resulted in the formation of the single-sided product, just like water [187] as shown previously. The stepwise synthetic protocol rules out the possibility of formation of any symmetric byproduct. Furthermore, the order in which the tris-ligands are attached does not have any effect on the outcome of the formed product. Instead asymmetric products were formed in both cases. Compared to previously reported methods for the isolation of asymmetric products explored for the $Mn^{III}Mo_6$ system [85, 184], this and similar procedures [171] are more controllable since it does not rely on re-arrangement of octamolybdate, save time, give high purity and good yield [188]. Further *post*-functionalization on asymmetrically functionalized POMs (**Figure 7, B5**) can be selective depending on *e.g.* the available functional groups that have been attached and the coupling reagent used. It is also possible to attach tris-ligands where one of the three hydroxyl groups has been exchanged with a carboxylic group [189]. The single-side decoration with tris-ligands breaks down the rather high symmetry in the parent Anderson-Evans cluster and the mixed enantiomers formed can be separated [102] in mixed organic solvents such as 60/40 DMF/MeCN (v/v) upon small additions of TBA-Br.

4.2.2.3 Synthesis of single and double-sided χ-isomers

Wei et al. recently activated the μ_2-O (**Figure 1A**) atoms (**Figure 7, C1**) in the Anderson-Evans cluster to form μ_2-OH by refluxing Anderson-Evans clusters in acidified aqueous solvent either separately or in the presence of the tris-ligand to be grafted (**Figure 7, C1-C2**). The activated proton allowed grafting of tris-NH_2, tris-CH_3 and tris-CH_2CH_3 ligands that cap a tetrahedral cavity instead of the heteroatom by covalently binding to two μ_3-O atoms and one μ_2-O atom on the planar Anderson-Evans surface giving the single-sided χ-isomer [190]. The formed product allows in theory further *post*-functionalization (**Figure 7**, **C3**) as observed with δ-isomers (**section 5.2**). Interestingly, when Zn^{II} and Ni^{II} were used as heteroatoms and tris-CH_3 and tris-CH_2OH as organic ligands, double-sided χ-isomers were also obtained despite using the route involving re-arrangement of octamolybdate (**Figure 7, C4**) which resulted in loss of the threefold symmetry [86].

5. Organic-inorganic Anderson-Evans POMs: The expandable world of hybrid structures

5.1 An overview of "extended" organic-inorganic structures

There exist 177 crystal structures of "extended" (**see section 2.2**) structures in the $Al^{III}Mo_6$ [61, 69, 74, 76-78, 81, 82, 173, 191-205], $Cr^{III}Mo_6$ [56, 60, 63, 65-69, 73, 76, 79, 81, 173, 177, 191, 194, 195, 199, 201, 204, 206-217], $Ni^{II}Mo_6$ [93, 175, 218-220], $Co^{II/III}Mo_6$ [221-223] $Fe^{III}Mo_6$ [224], $Cu^{II}Mo_6$ [174, 225-229], $Zn^{II}Mo_6$ [230], $As^{III}Mo_6$ [229-232], Mo_7 [112, 176, 193, 233-245], $Te^{VI}Mo_6$ [70, 246-250], $Te^{VI}W_6$ [70, 75, 251-253], $I^{VII}Mo_6$ [82, 97, 193, 214, 254-257], W_7 [172, 258], $Pt^{IV}Mo_6$ [259, 260] and $Pt^{IV}W_6$ [261] systems as of March 2015. The following paragraphs looks into some interesting organic-inorganic compounds in terms of structure and crystal packing.

A total of 25 crystal structures containing organic-inorganic aluminohexamolybdates exist as of March 2015 exhibiting various unusual topologies. Shivaiah et al. [203] have managed to crystallize $Cu_2(phen)_2(CH_3COO)(CH_3COOH)(H_2O)_2[Al(OH)_6Mo_6O_{18}] \times 28H_2O$, which incorporates a water pipe from solely lattice water molecules. There are 13 lattice water molecules involved in the water tube, forming an inner diameter of 8.527×8.061 Å^2. The Anderson-Evans cluster and the copper dimeric complex play an important role in the stabilization of the water pipe. Other reports from the same research group includes the novel chainlike coordination polymer $[Cu^{II}(2,2'\text{-bipy})(H_2O)_2Al(OH)_6Mo_6O_{18}]_n^{n-}$ [202] and $[Al(OH)_6Mo_6O_{18}\{Cu(phen)(H_2O)_2\}_2][Al(OH)_6Mo_6O_{18}\{Cu(phen)(H_2O)Cl\}_2] \times 5H_2O$ [201], where two polyoxometalate-supported copper phenanthroline complexes with different charge are crystallized to a neutral compound.

The properties of "extended" structures are strongly dependent on the choice of ligands since they give access to various topologies, especially porosities and cavities of different size forming highly dimensional structures. Wang and co-workers have combined ligands that do not exhibit SMM behavior with Anderson-Evans POMs in order to form new SMM materials (**section 6.5**) [82]. The compound $[\{CuTb(sal\text{-}3\text{-}met)(H_2O)_2\}_2\{AlMo_6O_{18}(OH)_6\}_2]$ exhibits SMM properties and is composed of two cationic $[CuTbL(H_2O)_3]^{3+}$ units and two $[AlMo_6O_{18}(OH)_6]^{3-}$ anions. Two {CuTb} moieties are covalently connected with two B-type Anderson-Evans POM units, forming a ring-type POM-supported heterometallic complex as shown in **Figure 8A**. This is one of the few examples, where the covalent attachment occurs with metals onto the terminal oxygen atoms and not by a functionalized tris-molecule capping μ_2 and/or μ_3-O atoms (see **Figure 1A**). Structure analogues were also successfully obtained with $[IMo_6O_{24}]^{5-}$ [82].

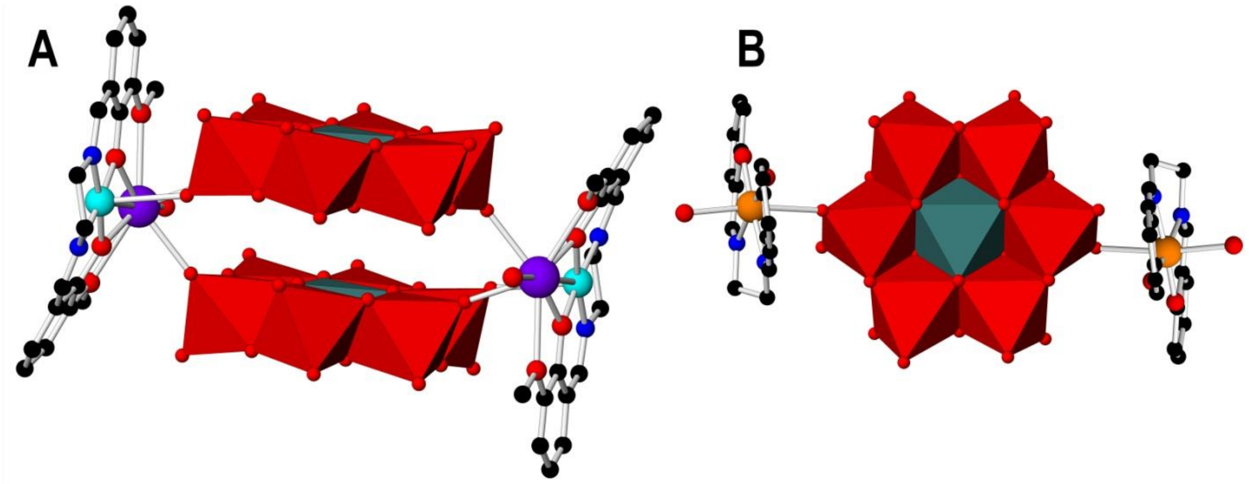

Figure 8. Combined ball-and-stick and polyhedral representation of [{CuTb(sal-3-met)$(H_2O)_2\}_2\{AlMo_6O_{18}(OH)_6\}_2]$ (**A**) and {Mn(salen)$_2(H_2O)_2[AlMo_6(OH)_6O_{18}]\}^-$ (**B**). Both structures feature covalent attachment on the unusual μ-O site in the Anderson-Evans POM. Red octahedra: Mo, Green octahedra: Al, cyan spheres: Cu; purple spheres: Tb; black spheres: C; orange spheres: Mn; blue spheres: N; red spheres: O. Hydrogen atoms and solvent molecules are omitted for clarity.

The introduction of specific $\{Mn^{III}_2\}$-Schiff base complexes also induces SMM behavior in the similar complexes Mn(salen)$_2(H_2O)_2[AlMo_6(OH)_6O_{18}]$ × arg × $20H_2O$ (**Figure 8B**) and Mn(salen)$_2(H_2O)_2[CrMo_6(OH)_6O_{18}]$ × arg × $11H_2O$, prepared by Wu et al. [81]. In the two compounds the Mn-Schiff bases are also covalently bonded to the terminal oxygen atoms of the $[AlMo_6(OH)_6O_{18}]^{3-}$ anion. The crystal structure revealed π-π interactions in between adjacent $\{Mn_2\}$ complexes in a staggered fashion with distances of 3.75 to 3.65 Å which is not observed in the similar [Mn(salen-am)$(H_2O)]_2Na[XMo_6(OH)_6O_{18}]$ × $20H_2O$ (X = Al, Cr) [204] compound.

Only a few $Cu^{II}/Zn^{II}Mo_6$ (7 and 5 crystal structures as of March 2015, respectively) compounds incorporating organic ligands have been reported based on both hydrothermal synthesis and conventional refluxing [225, 226, 230]. Interestingly, independently on the presence of organic counterpart, they all incorporate cyclic As_3O_6 trimers that are capping the Cu/ZnO_6 octahedron on both sides of the Anderson-Evans cluster. The incorporation of the As_3O_6 trimers has also been noted in the $Co^{II}Mo_6$ system [221]. The As_3O_6 unit can further be split up into three AsO_3 trigonal pyramids linked in a triangular arrangement by sharing corners with each other and corners in the Cu/ZnO_6 octahedron as shown in **Figure 9**. One reason for the attachment of the As_3O_6 in the formation of organic-inorganic Anderson-Evans compounds in the $Co^{II}Mo_6$, $Cu^{II}Mo_6$ and $Zn^{II}Mo_6$ systems may be related to the larger ionic radius of the heteroatoms resulting in an increase of the average X-(μ_3-O) (X = heteroatom) distance (**Table 1**). This causes an outwards expansion of the central XO_6 unit which the As_3O_6 trimers can stabilize.

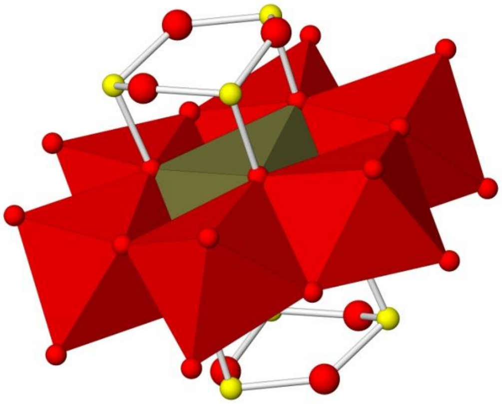

Figure 9. Combined ball-and-stick and polyhedral representation of $[As_6XMo_6O_{30}]^{4-}$ (X = Cu/Zn), the typical anion formed in reported organic-inorganic compounds of the $Cu^{II}Mo_6$ and $Zn^{II}MO_6$ systems [225, 226, 230]. Red octahedra: Mo, brown octahedron: Cu/Zn; yellow spheres: As; red spheres: O. Countercations and solvent molecules are removed for clarity.

5.2 An overview of tris-functionalized hybrid structures

Table 2 shows hybrid tris-functionalized crystal structures that contain the Anderson-Evans structure. The covalent attachment has explicitly been decorated with a wide variety of tris-ligands through either *pre* or *post*-functionalization using different procedures yielding symmetric and asymmetric products (see **Figure 7**). The variation in tris-ligands includes alkyl chains of differing lengths, aromatic ligands, ligands with remote binding sites and ligands with terminated functional groups such as amines and carboxylic acids. The following paragraphs looks into some interesting hybrid tris-functionalized compounds in terms of structure and crystal packing with a special emphasis on the $Mn^{III}Mo_6$ system.

Table 2. Tris-functionalized hybrid organic-inorganic compounds containing the Anderson-Evans anion in the crystal structure and structural/geometrical information on the grafting of the tris-ligand. The structures are arranged in an increasing atomic number for the templating heteroatom and under each XMo_6 system the structures are given in a chronological order with the oldest crystal structures first.

Compound	**tris-R* / single (S), double-sided (D), asymmetric double-sided (AS)**	**application****	**Ref**
$Al^{III}Mo_6$			
$[N(C_4H_9)_4]_3[AlMo_6O_{18}(OH)_3\{(OCH_2)_3CNHCH_2COOH\}] \times 10H_2O$	$-CH_2COOH$ (S)	nr	[262]
$[N(C_4H_9)_4]_3[AlMo_6O_{18}(OH)_3\{(OCH_2)_3CCH_2CH_3\}] \times 11H_2O$	$-CH_2CH_3$ (S)	nr	[262]
$[N(C_4H_9)_4]_3[AlMo_6O_{18}(OH)_3\{(OCH_2)_3CNH_2\}] \times 7H_2O$	$-NH_2$ (S)	nr	[262]
$[N(C_4H_9)_4]_3[AlMo_6O_{18}(OH)_3\{(OCH_2)_3CCH_2OH\}] \times 13H_2O$	$-CH_2OH$ (S)	nr	[262]
$[(C_4H_9)_4N]_3[AlMo_6O_{18}(OH)_3\{(OCH_2)_3CNHCOCH_2C_6H_4NNC_6H_5\}]$	$- NHCOCH_2C_6H_4NNC_6H_5$ (S)	photochromic, chiral transfer	[186]
$[TBA]_6\{[C_2H_5C(CH_2O)_3]AlMo_6O_{18}[(OCH_2)_3CNH_2]\}_2 \times 3DMF$	$-CH_2CH_3$, $-NH_2$ (AD)	nr	[188]
$[TBA]_3\{[C_2H_5C(CH_2O)_3]AlMo_6O_{18}(OH)_3\} \times [TBA]Br$	$-CH_2CH_3$ (S)	nr	[188]
$Cr^{III}Mo_6$			
$[(C_4H_9)_4N]_5\{H_7[HOCH_2C(CH_2)_3(CrO_6)Mo_6O_{18}]_2\}$	$-CH_2OH$ (S)	nr	[187]
$[(C_4H_9)_4N]_3[(C_2H_5)_3NH](CH_3CO_2H)Cl\{H_3[(CrO_6)Mo_6O_{18}(CH_2)_3CCH_2OH]\}$	$-CH_2OH$ (S)	nr	[187]
$(TBA)_3\{Cr(OH)_3Mo_6O_{18}[(OCH_2)_3CCH_2OH]\} \times 12H_2O$	$-CH_2OH$ (S)	nr	[171]
$(TBA)_3\{Cr(OH)_3Mo_6O_{18}[(OCH_2)_3CCH_3]\} \times 11H_2O$	$-CH_3$ (S)	nr	[171]
$(TBA)_3\{CrMo_6O_{18}[(OCH_2)_3CCH_2OH][(OCH_2)_3CCH_3]\}$	$-CH_2OH$, $-NH_2$ (AD)	nr	[171]
$[TBA]_3\{[CH_3C(CH_2O)_3]_2CrMo_6O_{18}\} \times 2DMF$	$-CH_3$ (D)	nr	[189]
$[TBA]_3\{[CH_3C(CH_2O)_2(COO)]_2CrMo_6O_{18}\} \times DMF$	tris$COCH_3$ (D)	nr	[189]
$[TBA]_3\ [H_2NC(CH_2O)_3]_2\{[H_3NC(CH_2O)_3]CrMo_6O_{18}(OH)_3\} \times 6H_2O$	$-NH_2$ (S)	nr	[102]
$[TBA]_3\{[H_2NC(CH_2O)_3CrMo_6O_{18}(OH)_3\} \times [TBA]Br \times 2H_2O$	$-CH_3$ (S)	nr	[102]
$[TBA]_3\{[H_3CC(CH_2O)_3CrMo_6O_{18}(OH)_3\} \times 4H_2O$	$-CH_3$ (S)	nr	[102]

$[TBA]_3\{[H_3CC(CH_2O)_3CrMo_6O_{18}(OH)_3\} \times 11H_2O$	$-CH_3$ (S)	nr	[102]
$[TBA]_3\{[H_3CNC(CH_2O)_3CrMo_6O_{18}(OH)_3\} \times [TBA]Br$	$-CH_3$ (S)	nr	[102]
$[TBA]_3\{[H_5C_2C(CH_2O)_3]CrMo_6O_{18}(OH)_3\} \times [TBA]Br \times NH_4Br$	$-CH_2CH_3$ (S)	nr	[102]
$[TBA]_3\{[H_2NC(CH_2O)_3]CrMo_6O_{18}(OH)_3\} \times [TBA]Br \times NH_2$	$-NH_2$ (S)	nr	[102]
$[TBA]_3\{[H_2NC(CH_2O)_3]CrMo_6O_{18}(OH)_3\} \times [TBA]Br \times 2H_2O$	$-NH_2$ (S)	nr	[188]
$[TBA]_3\{[H_5C_2C(CH_2O)_3]CrMo_6O_{18}(OH)_3\} \times [TBA]Br \times NH_4Br$	$-CH_2CH_3$ (S)	nr	[188]
$[TBA]_6\{[C_2H_5C(CH_2O)_3]CrMo_6O_{18}[(OCH_2)_3CNH_2]\}_2 \times 3DMF$	$-CH_2CH_3$, $-NH_2$ (AD)	nr	[188]
$[TBA]_2[H]\{[H_2NC(CH_2O)_3]CrMo_6O_{18}(OH)_3\}$	$-NH_2$ (S, χ-isomer)	nr	[190]
$[TBA]_2[H]\{[H_3CC(CH_2O)_3]\ CrMo_6O_{18}(OH)_3\}$	$-CH_3$ (S, χ-isomer)	nr	[190]
$[TBA]_2[H]\{[H_5C_2C(CH_2O)_3]\ CrMo_6O_{18}(OH)_3\}$	$-CH_2CH_3$ (S, χ-isomer)	nr	[190]
$[TBA]_2[H]\{[HOH_2CC(CH_2O)_3]\ CrMo_6O_{18}(OH)_3\}$	- CH_2OH (S, χ-isomer)	nr	[190]
$Mn^{III}Mo_6$			
$[TBA]_3[MnMo_6O_{18}\{(OCH_2)_3CNO_2\}_2] \times 2DMF$	$-NO_2$ (D)	nr	[86]
$[N(C_4H_9)_4]_3[MnMo_6O_{18}\{(OCH_2)_3CNH_2\}_2]$	$-NH_2$ (D)	nr	[263]
$[N(C_4H_9)_4]_3[MnMo_6O_{18}\{(OCH_2)_3CN{=}C(2\text{-}C_5H_4N)\}_2]$	$-N{=}C(2\text{-}C_5H_4N)$ (D)	nr	[263]
$[N(C_4H_9)_4]_3[MnMo_6O_{18}\{(OCH_2)_3CN{=}C(4\text{-}C_5H_4N)\}_2]$	$-N{=}C(4\text{-}C_5H_4N)$ (D)	Photocatalysis, Ag^+ recovery	[263]
$[(C_4H_9)_4N]_3[MnMo_6O_{18}\{(OCH_2)_3CNHCO(4\text{-}C_5H_4N)\}_2] \times (CH_3CN)_4$	$-N{=}C(4\text{-}C_5H_4N)$ (D)	self-assembly of an anisotropic gel	[264]
$(ET)_5\{MnMo_6O_{18}[(OCH_2)_3CCH_2OH]_2\} \times 5H_2O$	$-CH_2OH$ (D)	nr	[265]
$(ET)_5\{MnMo_6O_{18}[(OCH_2)_3CCH_2CH_3]_2\} \times 2MeCN$	$-CH_2CH_3$ (D)	semiconducting	[265]
$(ET)_6\{MnMo_6O_{18}[(OCH_2)_3CNH_2]_2\} \times 2CH_2Cl_2$	$-NH_2$ (D)	nr	[265]
$[N(C_4H_9)_4]_3[MnMo_6O_{18}\{(OCH_2)_3CNH\text{-}CH_2\text{-}C_{16}H_9\}_2] \times 2\ DMF \times 3\ H_2O$	$-NH\text{-}CH_2\text{-}C_{16}H_9$(D)	absorbent of organic solvents	[181]
$\{Ag_3[MnMo_6O_{18}\{(OCH_2)_3CNH_2\}_2(DMSO)_5] \times 3(DMSO)\}_n$	$-NH_2$ (D)	fiber formation	[266]
$\{Ag_3[MnMo_6O_{18}\{(OCH_2)_3CNH_2\}_2(DMSO)_6(CH_3CN)_2] \times DMSO\}_n$	$-NH_2$ (D)	fiber formation	[266]
$[(nC_4H_9)_4N]_3[MnMo_6O_{18}\{(OCH_2)_3CNH\text{-}CO\text{-}(CH_2)_4CH_3\}_2] \times 2DMF$	$-NHCO(CH_2)_4CH_3$ (D)	encapsulation by surfactants	[267]
$[(nC_4H_9)_4N]_3[MnMo_6O_{18}\{(OCH_2)_3CNH\text{-}CO\text{-}(CH_2)_{14}CH_3\}_2] \times 7H_2O \times 2DMF$	$-NHCO(CH_2)_{14}CH_3$ (D)	encapsulation by surfactants	[267]
$[n\text{-}(C_4H_9)_4N]_3[MnMo_6O_{18}\{(OCH_2)_3C\text{-}NO_2\}\{(OCH_2)_3C\text{-}NH_2\}] \times 2DMF$	$-NO_2$, $-NH_2$ (AD)	nr	[184]
$[n\text{-}(C_4H_9)_4N]_3[MnMo_6O_{18}\{(OCH_2)_3C\text{-}NO_2\}\{(OCH_2)_3C\text{-}N{=}CH(C_5H_4N)\}]$	$-NO_2$, $-N{=}C(4\text{-}C_5H_4N)$ (D)	nr	[184]
$[TBA]_3[MnMo_6O_{24}C_{34}H_{41}N]$	$-(CH_2)_8CH_3$ (D)	nanofiber formation	[183]
$[TBA]_3[MnMo_6O_{24}C_{26}H_{46}] \times 2(CH_3CN)$	$-(CH_2)_8CH_3$, $-NH\text{-}CH_2\text{-}C_{16}H_9$ (AD)	nanofiber formation	[183]
$(TBA)_3[MnMo_6O_{18}\{(OCH_2)_3CN = CH\text{-}C_6H_5\}_2]$	$-NCH\text{-}C_6H_5$ (D)	nr	[268]
$(TBA)_3[MnMo_6O_{18}\{(OCH_2)_3CN = CH\text{-}C_6H_5O\}_2]$	$-NCH\text{-}C_6H_4\text{-}OH$ (D)	nr	[268]
$(TBA)_3[MnMo_6O_{18}\{(OCH_2)_3CN = CH\text{-}C_{11}H_8N\}_2]$	$-NCH\text{-}C_6H_4\text{-}C_5NH_5$ (D)	nr	[268]
$(TBA)_3[MnMo_6O_{18}\{(OCH_2)_3CN = CH\text{-}C_{13}H_9\}_2]$	$-NCH\text{-}C_6H_4\text{-}C_{13}H_9$ (D)	nr	[268]
$(TBA)_7[Mo_6O_{18}NC(OCH_2)_3MnMo_6O_{18}(OCH_2)_3CNMo_6O_{18}]$	$-N\text{-}Mo_6O_{18}$ (D)	nr	[269]
$[C_{16}H_{36}N]_3[C_{40}H_{34}N_8O_{26}MnMo_6] \times C_3H_7NO_3C_4H_9NO$	$-NH\text{-}C_{40}H_{33}N_7$ (D)	POM-photosensitizer complexaction	[270]
$(TBA)_3[MnMo_6O_{18}\{(OCH_2)_3CNC_{25}H_{34}N_2O_2\}_2]$	- $NH\text{-}C_{25}H_{33}N_2O_2$ (D)	photochromic upon UV radiation	[271]
$(TBA)_3[MnMo_6O_{18}\{(OCH_2)_3CNHC_9H_{10}\}_2]$	$-NH\text{-}$ C_9H_{10} (D)	photochromic upon UV radiation	[271]
$(TMA)_3[MnMo_6O_{18}((OCH_2)_3CNH_2)_2]$	$-NH_2$ (D)	nr	[178]
$(TEA)_3[MnMo_6O_{18}((OCH_2)_3CNH_2)_2]$	$-NH_2$ (D)	nr	[178]
$(TPA)_2Na_1[MnMo_6O_{18}((OCH_2)_3CNH_2)_2]$	$-NH_2$ (D)	nr	[178]
$Na_3[MnMo_6O_{18}((OCH_2)_3CNH_2)_2]$	$-NH_2$ (D)	nr	[178]
$(TBA)_7[H_{10}C_8NMo_6O_{18}NC(OCH_2)_3MnMo_6O_{18}(OCH_2)_3CNMo_6O_{18}NC_8H_{10}]$	$-NMo_6O_{18}NC_8H_{10}$ (D)	nr	[272]
$(TBA)_7[H_{13}C_9NMo_6O_{18}NC(OCH_2)_3MnMo_6O_{18}(OCH_2)_3CNMo_6O_{18}NC_9H_{13}]$	$-NMo_6O_{18}NC_9H_{13}$ (D)	nr	[272]
$(TBA)_3[MnMo_6O_{18}\{(OCH_2)_3C\text{-}NHCOCH_2C_5N_5H_4\}_2]$	$-NHCO\text{-}CH_2\text{-}C_5N_5H_4$ (D)	thermal-induced self-assembly	[273]
$(TBA)_3\{MnMo_6O_{18}[(OCH_2)_3CNHCOC_6H_4FeC_{10}H_9]_2\}$	$-NHCO\text{-}C_6H_4\text{-}FeC_{10}H_9$ (D)	self-assembly of spherical morphologies	[274]
$(TBA)_3[MnMo_6O_{18}\{(OCH_2)_3CNH_2\}\{(OCH_2)_3CNHC_{21}H_{19}N_2O_4\}]$	$-NH\text{-}C_{21}H_{19}N_2O_4$ (D)	photochromic upon UV/visible light	[185]
$[TBA]_3[(MnMo_6O_{18})((OCH_2)_3\text{-}C\text{-}(CH_2)_7CHCH_2)_2]$	$-(CH_2)_7CHCH_2$ (D)	nr	[182]
$[PPh_4]_3[(MnMo_6O_{18})((OCH_2)_3C\text{-}NHCH_2C_{16}H_9)_2]$	$-NHCH_2C_{16}H_9$ (D)	nr	[182]
$[TBA]_3[(MnMo_6O_{18})((OCH_2)_3C\text{-}NHC(O)CH_2CHCH_2)_2]$	$-NHCOCH_2CHCH_2$ (D)	nr	[182]
$[TBA]_3[(MnMo_6O_{18})((OCH_2)_3C\text{-}NHC(O)(CH_2)_{10}CH_3)_2])$	$-NHCO\text{-}(CH_2)_{10}CH_3$ (D)	nr	[182]
$[TBA]_3[(MnMo_6O_{18})((OCH_2)_3C\text{-}NHC(O)(CH_2)_{18}CH_3)_2])$	- $NHCO\text{-}(CH_2)_{18}CH_3$ (D)	nr	[182]
$[n\text{-}(C_4H_9)_4N]_3[MnMo_6O_{24}(C_{19}H_{16}NO)(C_4H_8N)] \times 3DMF$	$-NH_2$, $-NHCO\text{-}C_{19}H_{15}$ (D)	nr	[85]
$[n\text{-}(C_4H_9)_4N]_3[MnMo_6O_{24}(C_{19}H_{18}NO_2)(C_4H_8N)] \times 3DMF$	$-C_{19}H_{18}NO_2$ (D)	nr	[85]
$[n\text{-}(C_4H_9)_4N]_3[MnMo_6O_{24}(C_7H_{12}NO)(C_4H_8N)] \times 3DMF$	$-C_7H_{12}NO$ (D)	nr	[85]
$[n\text{-}(C_4H_9)_4N]_3[MnMo_6O_{24}(C_{19}H_{16}NO)_2] \times 3MeCN$	$-C_{19}H_{16}NO$ (D)	nr	[85]
$(TBA)_3[MnMo_6O_{18}((OCH_2)_3CNHCOCH_2CH_3)_2]$	$-NHCOC_{19}H_{15}$ (D)	nr	[275]
$(TBA)_3[MnMo_6O_{18}((OCH_2)_3CNHCOC_6H_5)_2]$	$-NHCOC_6H_5$ (D)	nr	[275]
$(TBA)_3[MnMo_6O_{18}((OCH_2)_3CNHCO(C_4H_9)_4)_2]$	$-NHCO(C_4H_9)_4$ (D)	nr	[275]
$(TBA)_3[MnMo_6O_{18}((OCH_2)_3CNHCOCH_2CH_2COOH)_2]$	$-NHCOCH_2CH_2COOH$ (D)	nr	[275]
$(TBA)_3[MnMo_6O_{18}((OCH_2)_3CNHCOCH_2CH_2CH_2COOH)_2]$	$-NHCOCH_2CH_2CH_2COOH$ (D)	nr	[275]
$(TBA)_3[MnMo_6O_{18}((OCH_2)_3CNHCOC_4H_8COOH)_2]$	$-NHCOC_4H_8COOH$ (D)	nr	[275]
$(TBA)_3[MnMo_6O_{18}((OCH_2)_3CNHCOC_6H_4COOH)_2]$	$-NHCOC_6H_4COOH$ (D)	nr	[275]
$(TBA)_3[MnMo_6O_{18}((OCH_2)_3CNHCOC_{30}H_{20}COOH)_2]$	$-NHCOC_{30}H_{20}COOH$ (D)	nr	[275]
$(TBA)_3[MnMo_6O_{24}(C_{12}H_{15}N_2O_5)_2] \times 4DMF$	$-C_{12}H_{15}N_2O_5$ (D)	POM-peptide integration	[276]
$(TBA)_3[MnMo_6O_{24}(C_{17}H_{21}N_2O_4)_2] \times 4DMF$	$-C_{17}H_{21}N_2O_4$ (D)	POM-peptide integration	[276]
$[TBA]_3\{[H_2NC(CH_2O)_3]MnMo_6O_{18}(OH)_3\} \times [TBA]Br$	$-NH_2$ (S)	nr	[188]
$[TBA]_6\{[C_2H_5C(CH_2O)_3]MnMo_6O_{18}[(OCH_2)_3CNH_2]\}_2 \times 4DMF$	$-CH_2CH_3$, $-NH_2$ (AD)	nr	[188]
$[TBA]_2[H]\{[H_2NC(CH_2O)_3]MnMo_6O_{18}(OH)_3\}$	$-NH_2$ (S, χ-isomer)	nr	[190]
$Fe^{III}Mo_6$			
$(TBA)_3[FeMo_6O_{18}\{(OCH_2)_3CNH_2\}_2]$	$-NH_2$ (D)	nr	[263]
$(TBA)_3[FeMo_6O_{18}\{(OCH_2)_3CNHCO(4\text{-}C_5H_4N)\}_2]$	$-NH\text{-}(4\text{-}C_5H_4N)$ (D)	nr	[277]
$(TBA)_7[Mo_6O_{18}NC(OCH_2)_3FeMo_6O_{18}(OCH_2)_3CNMo_6O_{18}]$	- NMo_6O_{18} (D)	nr	[269]
$Na_3[FeMo_6O_{18}\{(OCH_2)_3CCH_2OH\}_2] \times 11\ H_2O$	$-CH_2\text{-}OH$ (D)	protein charge inversion	[57]
$Na[TMA]_2[FeMo_6O_{18}(OH)_3\{(OCH_2)_3CNH_3\}](OH) \times 6\ H_2O$	$-NH_3^+$ (S)	protein charge inversion	[57]
$Ni^{II}Mo_6$			

$[TBA]_3[H_2NiMo_6O_{18}\{(OCH_2)_3CNO_2\}_2]$	$-NO_2$ (D, χ-isomers)	nr	[86]
$Zn^{II}Mo_6$			
$[TBA]_3[H_2ZnMo_6O_{18}\{(OCH_2)_3CCH_3\}_2]$	$-CH_3$ (D, χ-isomers)	nr	[86]
$Ga^{III}Mo_6$			
$[TBA]_3[GaMo_6O_{18}(OH)_3\{(OCH_2)_3CCH_2OH\}] \times 12\ H_2O$	$-CH_2OH$ (S)	protein charge inversion	[57]
$[TMA]_2[GaMo_6O_{18}(OH)_3\{(OCH_2)_3CNH_3\}] \times 7\ H_2O$	$-NH_3^+$ (S)	protein charge inversion	[57]

*δ-isomer unless else stated, **nr = not reported

As of March 2015, 21 crystal structures of hybrid tris-functionalized $Cr^{III}Mo_6$ compounds exist. The $Cr^{III}Mo_6$ has functioned as a model system that has been decorated with small tris-ligands (tris-CH_3, tris-CH_2CH_3, tris-CH_2OH and tris-NH_2) in order to explore new synthesis protocols (see **Figure 7**). Wu et al. [187] recently reported the first single-side tris-functionalized Anderson-Evans POM that contains covalently attached tris-CH_2-OH to a $Cr^{III}Mo_6$ unit (**Figure 7, B2**). The single-side functionality allows the formation of the dimeric complex $[(C_4H_9)_4N]_5\{H_7[HOCH_2C(CH_2)_3(CrO_6)Mo_6O_{18}]_2\}$ that is held together by seven hydrogen bonds between the undecorated sides. The dimeric complexes align their plane in an off center parallel orientation (**Figure 10**). The dimer can be split to obtain monomers resulting in the $\{H_3[(CrO_6)Mo_6O_{18}(CH_2)_3CCH_2OH]\}^{3-}$ anion. A similar interaction between the undecorated sides in the $Ga^{III}Mo_6$ system has also been noted [57].

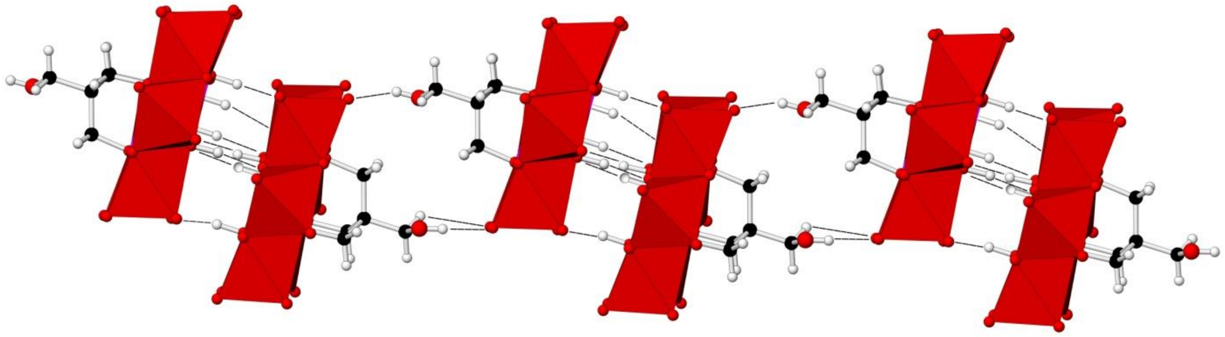

Figure 10. The extensive network of hydrogen bonds that holds together the cross-linked $[(C_4H_9)_4N]_5\{H_7[HOCH_2C(CH_2)_3(CrO_6)Mo_6O_{18}]_2\}$ dimer units. Seven hydrogen bonds are present in between the undecorated sides and three additional hydrogen bonds are present in between tris-CH_2OH and terminal oxygen atoms in the next anion. Red octahedra: Mo; black spheres: C; red spheres: O; white spheres: H.

The $Mn^{III}Mo_6$ system is one of the best explored hybrid tris-functionalized organic-inorganic Anderson-Evans polyoxometalates and as of March 2015 60 crystal structures have been reported. The research group of Hasenknopf has since their first report on tris-functionalization successfully grafted 2-pyridinecarbaldehyde to $Mn^{III}Mo_6$ and $Fe^{III}Mo_6$ systems [263]. Other successfully attached ligands by the research group includes terpyridine ligands [270] and pendant pyridyl groups [277] resulting in the anions illustrated in **Figure 11A** and **B** offering remote binding sites (see **section 6.3**).

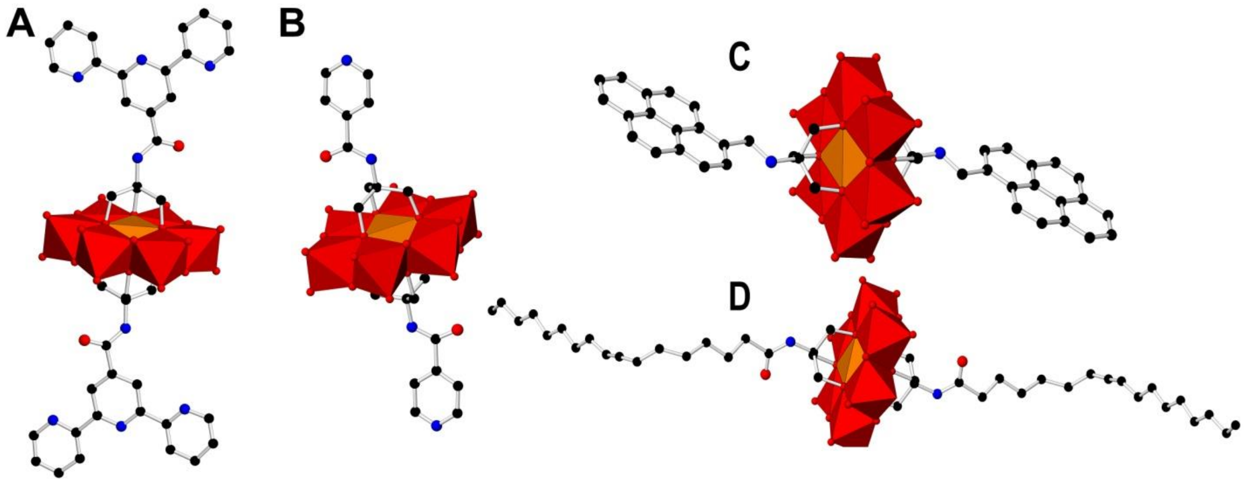

Figure 11. Combined ball-and-stick and polyhedral representation of $[MnMo_6O_{18}\{(OCH_2)_3CNHCO(C_{14}N_3H_{10})\}_2]^{3-}$ (**A**), $[MnMo_6O_{18}\{(OCH_2)_3CNHCO(4\text{-}C_5H_4N)\}_2]^{3-}$ (**B**), $[MnMo_6O_{18}\{(OCH_2)_3CNHCO(CH_2)_{15}CH_3\}_2]^{3-}$ (**C**) and $[MnMo_6O_{18}\{(OCH_2)_3CNH\text{-}CH_2\text{-}C_{16}H_9\}_2]^{3-}$ (**D**). Despite the similarity of the attached ligands in each anion the properties differ markedly resulting in specific applications. Red octahedra: Mo, orange octahedra: Mn; black spheres: C; blue spheres: N; red spheres: O. Hydrogen atoms are omitted for clarity.

The group of Cronin has reported on numerous different hybrid Anderson-Evans POMs mainly in the $Mn^{III}Mo_6$ system with different properties. As shown in **section 3**, the choice of cation linker can be of great importance for the physical properties of the entire compound which is applicable to hybrid systems as well. The presence of Ag^+ and DMSO is crucial for the thermal stability of tris-functionalized $[MnMo_6O_{18}\{(OCH_2)_3CNH_2\}_2(DMSO)_n]^{3-}$ anions despite different types of polymers and bridging modes present [266]. However, it is not only the cation linker that determines the geometrical and physical properties of the compounds but also the geometry of organic ligands that are *post*-functionalized. When anhydride precursors are used to *post*-functionalize the hybrid anion $[MnMo_6O_{18}((OCH_2)_3CNH_2)_2]^{3-}$ the reaction can be selective by the bulkiness of the anhydride used leading to the isolation of specific isomers [275]. If aromatic ligands are attached instead as in $[MnMo_6O_{18}\{(OCH_2)_3CNH\text{-}CH_2\text{-}C_{16}H_9\}_2]^{3-}$ that contains pyrene ligands (**Figure 11C**), nanoscale butterfly shaped channels in the crystal structure can be formed approximately 1 nm wide and 2 nm long. This interesting packing induced by the aromatic ligands is held together only by van der Waals and C-H ··· O-Mo hydrogen bonds and is stable up to 240 °C [181].

Rosnes et al. [182] have symmetrically attached alkyl chains of different lengths onto the $Mn^{III}Mo_6$ core ranging from C_4 to C_{20} *via* tris-like moieties (C_{17} shown in **Figure 11D**). The chain length affects the surface architecture giving rise to different fibrous assemblies with different heights. By introducing the correct mixture of POM-organic ligand and cation the self-assembly on surfaces can be controlled. The long alkyl chain can also self-assemble to form vesicles and is discussed in **section 6.1**. Several examples involving attachment of even larger units have been reported. Macdonell et al. [278] attached tris-ligands containing terminal alkyne and azide groups coupled to $Mn^{III}Mo_6$. A Cu-catalyzed alkyne−azide cycloaddition reaction was then applied to link the clusters together forming linear oligomers in the nanometer range. Yvon et al. [276] have reported on the $Mn^{III}Mo_6$ POM with 15 amino acids attached on each side of the POM. The modified properties of the inorganic diamine may be useful in both medical and nano-science research, in specific as recognition motifs and catalytically active sites where key amino acids may be replaced by POM amino acids. Schamming et al. [279] has reported on the synthesis of a hybrid POM-porphyrin copolymeric film with zinc octaethylporphyrin (**Figure 12**) and zinc 5,15-dipyridinium octaethylporphyrin in the presence of $[MnMo_6O_{18}\{(OCH_2)_3CNHCO(4\text{-}C_5H_4N)\}_2]^{3-}$ which can be used for metal recovery (**section 6.3**). Yuanchun et al. [190] have covalently attached $[MnMo_6O_{18}\{(OCH_2)_3CNH_2\}_2]^{3-}$ to carboxylic acid-functionalized single-walled carbon nanotubes by amide bond formation which can act as electrode material in lithium ion batteries.

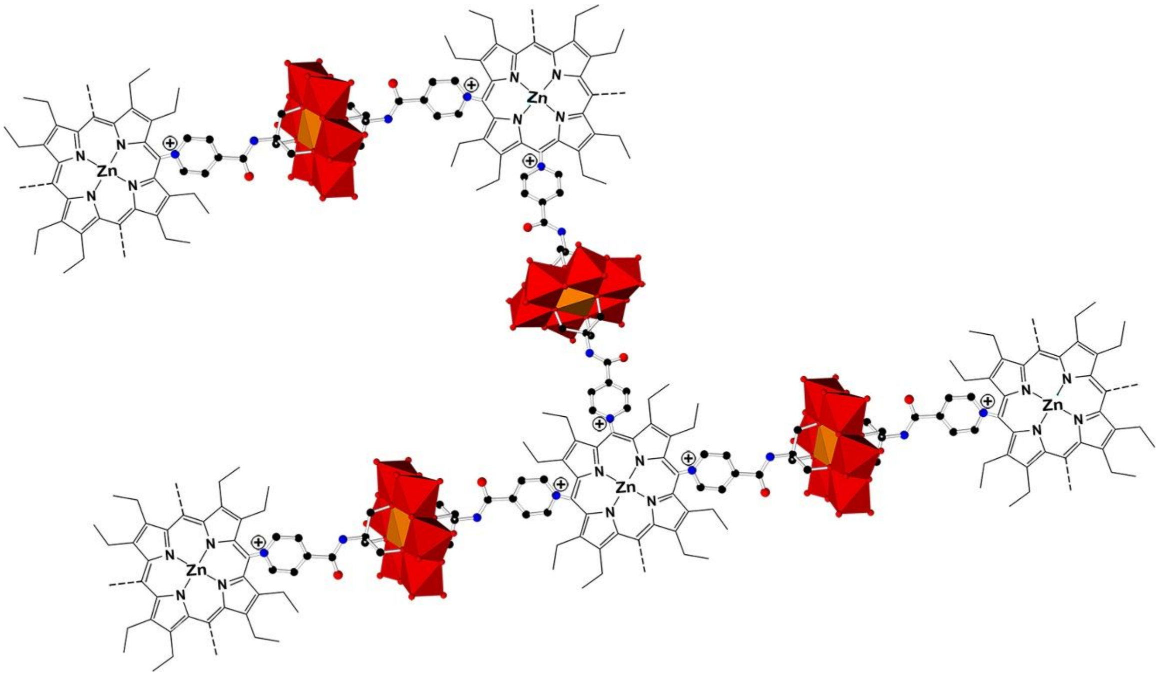

Figure 12. Representation of the hybrid coordination two-dimensional polymer obtained by electropolymerization of $[MnMo_6O_{18}\{(OCH_2)_3CNHCO(4\text{-}C_5H_4N)\}_2]^{3-}$ with zinc octaethylporphyrin. Red octahedra: Mo, orange octahedron: Mn; black spheres: C; blue spheres: N; red spheres: O; dark blue spheres: Zn. Hydrogen atoms are omitted for clarity.

Nanoscale POM-organic hybrid chiral molecular rods are one of the few examples where different POM archetypes are covalently linked *via* organic molecules. The $[Mo_6O_{18}NC(OCH_2)_3MnMo_6O_{18}(OCH_2)_3CNMo_6O_{18}]^{7-}$ anion shown in **Figure 13A** consists of two types of POMs, Anderson-Evans and Lindqvist. Two monosubstituted hexamolybdates are covalently bound to one imido ligand on each side of the organically modified Anderson-Evans POM. The compound crystallized as a chiral triad [269].

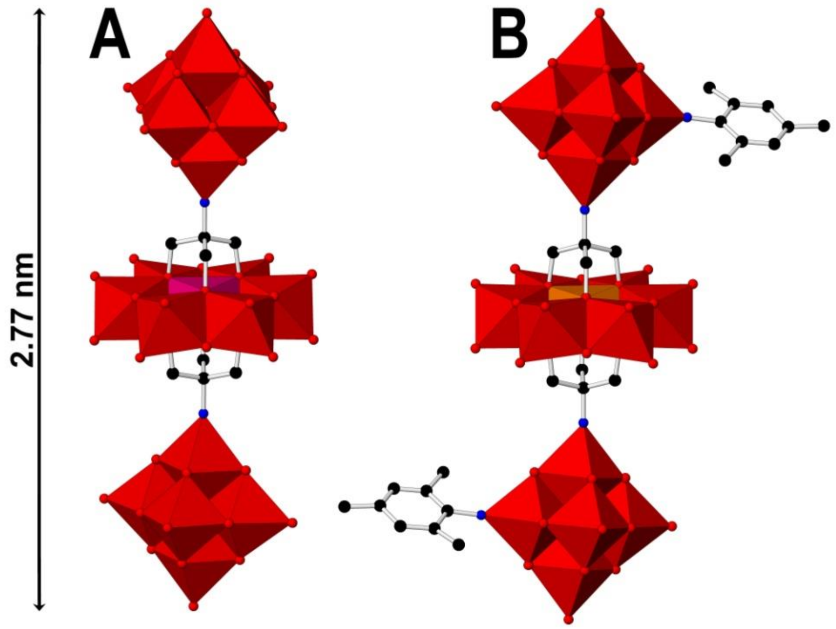

Figure 13. Combined ball-and-stick and polyhedral representation of $[Mo_6O_{18}NC(OCH_2)_3XMo_6O_{18}(OCH_2)_3CNMo_6O_{18}]^{7-}$ (X = Mn/Fe) (**A**) and $[C_9H_{11}NMo_6O_{17}NC(OCH_2)_3MnMo_6O_{18}(OCH_2)_3CNMo_6O_{17}NC_9H_{11}]^{7-}$ (**B**) which can be viewed as a nanorod that measures roughly 2.77 nm. Red octahedra: Mo, pink octahedron: Mn/Fe; orange octahedron: Mn; black spheres: C; blue spheres: N; red spheres: O. Hydrogen atoms are omitted for clarity.

The nanorod was further functionalized by attaching a variety of aryl-alkylimido ligands to terminal oxygen atoms of the hexamolybdates (**Figure 13B**). No π-π stacking exist between the phenyl rings that are attached to the hexamolybdate and the nanorod still measures roughly 2.77 nm but contains added "wings" on the sides [272].

Besides the versatile tris-functionalization in the $Cr^{III}Mo_6$ and $Mn^{III}Mo_6$ systems tris-decoration has been reported in $Zn^{II}Mo_6$ [86] (1 crystal structure as of March 2015) which was functionalized with tris-CH_3 yielding the χ-isomer (see **Figure 4A**). However, when tris-NH_2 was used instead in combination with Zn^{II} or Ni^{II} the anion $[Mo_2X_2O_6\{(OCH_2)C(NH_2)CH_2OH\}_2(CH_3CO_2)_2]^{2-}$ (X = Zn, Ni) was obtained. Due to the stronger affinity for nitrogen donors tetra- and pentacoordinate Zn/Ni atoms with N and O donor atoms and tetra- and hexacoordinate Mo atoms with O donor atoms was found instead [263]. The $I^{VII}Mo_6$ system contains 13 crystal structures as of March 2015 of which the majority involves non-covalent attachment of organic molecules. No tris-functionalization exists but when the $[IMo_6O_{24}]^{5-}$ anion is refluxed in acidic conditions it becomes protonated. Interestingly, the protonation occurs on μ_2-O atoms rather than at μ_3-O sites (see **Figure 1A**) which are the most basic oxygen atoms in the $[IMo_6O_{24}]^{5-}$ anion. The protonated molybdoperiodate can be methylated as shown in **Figure 14** by dissolving the protonated ion in a methanol solution [257]. This study is an important step towards covalent functionalization of A-type Anderson-Evans anions.

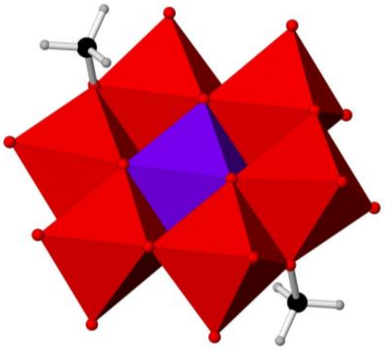

Figure 14. Combined ball-and-stick and polyhedral representation of $[IMo_6O_{22}(OCH_3)_2]^{3-}$ with one methylated μ_2-O atom on each side of the planar structure. Red octahedra: Mo; purple octahedron: I; black spheres: C; grey small spheres: H; red spheres: O. Counter cations and solvent molecules are removed for clarity.

6. Different uses of Anderson-Evans POMs

6.1 Nanomaterials: Self-assembly of amphiphillic organic-inorganic hybrid POMs

POMs across larger length scales form nanostructures that have significantly less ordered supramolecular interactions due to the increased number of free variables from the long organic chains. This gives room for interesting nanostructures compared to *e.g.* POM assembly at the molecular level. Alkyl C_6, C_{16} and C_{18} chains have been grafted onto the $Mn^{III}Mo_6$ system leading to the formation of hydrophilic-hydrophobic surface-grafted clusters and surfactant-encapsulated clusters in the nanometer range that are enclosed by surfactant DODA [267]. It also allows the formation of hydrophobic-hydrophilic-hydrophobic layers due to the planar form of the Anderson-Evans POM allowing grafting of organic ligands on both sides. Other POM archetypes that are bigger and bulkier can only form hydrophobic-hydrophilic layers. The planar surface of the Anderson-Evans POM still allows the alkyl chains to arrange themselves to the same side, at the right conditions, so that the alkyl chains point into the same direction (Figure 15). In fact, compounds of $Mn^{III}Mo_6$ with C_6 and C_{16} chains exhibit amphiphillic surfactant behavior in mixed solvents of acetonitrile and water and form membrane-like vesicles. The POM itself is used as polar head groups on the outside, whereas the long alkyl chains stay inside the spherical vesicle forming a bilayer structure (**Figure 15**) [280].

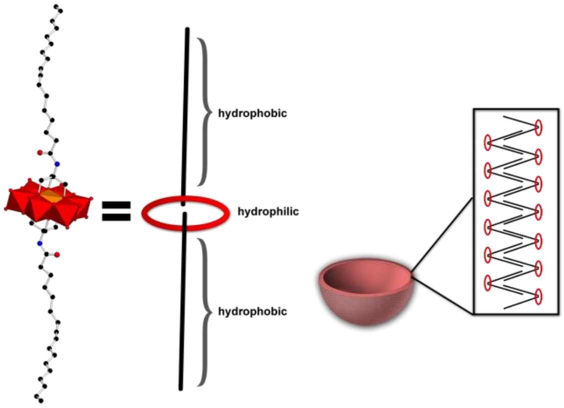

Figure 15. The packing arrangement of the hybrid $Mn^{III}Mo_6$ POM in order to form vesicles. Red octahedra: Mo, orange octahedron: Mn; black spheres: C; blue spheres: N; red spheres: O. Hydrogen atoms are omitted for clarity.

He et al. [273] found a thermal-induced dynamic self-assembly that also formed spherical structures depending on the chain length of cationic surfactants and the ambient temperature by grafting adeninyl groups onto the $Mn^{III}Mo_6$ Anderson-Evans cluster and encapsulating them by TBA and DODA. TBA cations induced fibrous, rod-like, and tubular architectures upon temperature increase, whereas the longer chains in DODA transformed from fibers to spheres upon heating. Both processes are reversible. The covalent attachment of ferrocene [274] instead of adeninyl groups results in a soft building block upon replacement of TBA with DODA that self-assemble into spherical aggregates from linear architectures. Thus, the formed complexes may be used to tune nanostructures containing POMs to obtain the desired properties in terms of size and morphology.

6.2 Anderson-Evans POMs with attached photochromic molecules

The ability to attach organic photochromic compounds [281] like spiropyran and azo compounds *via* either covalent or non-covalent attachment to the Anderson-Evans POM has resulted in the synthesis of new organic-inorganic compounds with enhanced photochromic properties. The photochromic compound spiropyran has been covalently attached single (**Figure 16A**) and double-sided to the $Mn^{III}Mo_6$ Anderson-Evans POM that resulted in efficient photochromic compounds with high coloration contrasts [185]. Non-covalent attachment of SP has been reported in the complexes $(SP)_2(H_3O)[X(OH)_6Mo_6O_{18}] \times H_2O \times 2CH_3CH_2OH$ ($X = Al^{III}$ and Fe^{III}) together with several other POM archetypes. The Anderson-Evans complexes was one of the complexes that improved the photocoloration contrast the best compared to some conventional POM clusters like Keggin and Lindqvist structures, which originates in the high-energy ligand-to-metal charge transfer (LMCT) giving a considerable shift close to the UV domain limiting the initial color of the samples [282]. Coué et al. [243] also reported photochromic properties with $(H_2DABCO)_2(NH_4)_2[Mo_7O_{24}]$ together with trimolybdate and octamolybdate derivatives. The compounds exhibit photochromic behavior upon UV excitation and their colors shift differently depending on which POM is present. The kinetics of the color change is determined by the organic component and its interface with the inorganic counterpart.

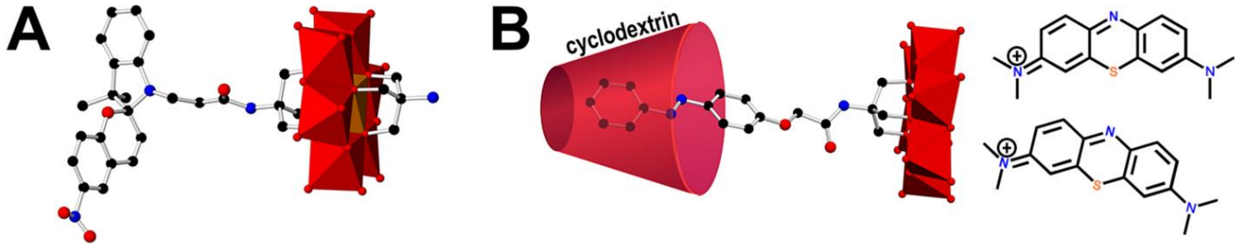

Figure 16. Combined ball-and-stick and polyhedral representation of $[MnMo_6O_{18}\{(OCH_2)_3CNH_2\}\{(OCH_2)_3CNHC_{21}H_{19}N_2O_4\}]^{3-}$ (**A**). Schematic illustration of the three component system used for the chiral recognition and transfer by the $[AlMo_6O_{18}(OH)_3(OCH_2)_3CHNCOCH_2OH_4C_6NNC_6H_5]^{3-}$ anion from cyclodextrin to MB (**B**). Red octahedra: Mo, orange octahedron: Mn; black spheres: C; blue spheres: N; red spheres: O; yellow spheres: S. Hydrogen atoms are omitted for clarity.

Another class of famous photochromic compounds are the azo compounds bearing the functional azo group R-N=N-R', which can either be in *trans* or *cis* conformation. The azo bond was studied in aliphatic chains with differing lengths, consisting of two phenyl units bridged by the azo bond and attached to the $Mn^{III}Mo_6$ core. Upon UV irradiation of the sample a conformational change from *trans* to *cis* occurred whereas exposure to visible light reversed the process [271]. The anion $[AlMo_6O_{18}(OH)_3(OCH_2)_3CHNCOCH_2OH_4C_6NNC_6H_5]^{3-}$ containing the single-side covalently attached aromatic azobenzene ligand has been studied in a three supramolecular hybrid system (POM - α-cyclodextrin - MB). It allows the chiral transfer based on host-guest recognition from the inner cavity of the α-cyclodextrin to phenyl groups in the *trans*-state of the azobenzene ligand. Electrostatic interaction between the free side of the POM and MB induces chirality in MB (**Figure 16B**) [186].

6.3 Photocatalytic properties

POMs can catalyze a variety of reactions such as organic reactions including alkene and alcohol oxidation, water splitting and site-specific cleavage of biomolecules. Several smaller inorganic clusters have proved to be efficient catalysts. Ammonium molybdate, $(NH_4)_6Mo_7O_{24} \times 4H_2O$, is an efficient and selective catalyst for the oxidation of thiols to corresponding disulfides using potassium bromate in a mixture of water and acetonitrile [283]. Tanaka et al. [284] found that the simple anion $[CoMo_6O_{24}H_6]^{3-}$ effectively catalyze (initial turnover frequency = 0.11 s^{-1}) the photoinduced water oxidation reaction forming O_2 in a system consisting of tris(2,2'-bipyridine)ruthenium(II) and sodium persulfate in comparison to other Co containing POMs. Control experiments revealed that presence of Co is essential for catalytic activity but also that Co metal centers with higher nuclearity in other POM archetypes are not necessary to attain high catalytic activity as the mononuclear Co center in the Anderson-Evans POM can also serve as O_2-evolving catalyst. The $(H_2DABCO)(HDABCO)[Fe(OH)_6Mo_6O_{18}]$ compound has also proved to be a good oxidation catalyst and forms together with $(H_2DABCO)_2(HDMA)_{0.5}Na_{0.75}(H_3O)_{0.75}[Mo_8O_{27}]$ one of the most efficient photochromic Mo-POM materials in regard to coloration contrast and coloration speed [224].

Several "extended" structures of $Al^{III}Mo_6$, $Cr^{III}Mo_6$ and $I^{VII}Mo_6$ systems have been subject for the photodegradation of RhB with UV irradiation and are summarized in **Table 3**. The degradation has been measured as the decrease in the UV-Vis signal at 554 nm, which is the absorption maximum of RhB and corresponds to $n \rightarrow \pi$ transition of C=N, C=O groups. Thus, the results in **Table 3** give a measure of the decolorization of the dye with time [285]. In comparison to other POM archetypes, several of the Anderson-Evans POMs in **Table 3** have a higher decrease in the UV signal than the Keggin $[SiW_{12}O_{40}]^{4-}$ anion [286] which was also tested for photodegradation of RhB. There seems to also be dependence between the catalytic conversion and the heteroatom present in the Anderson-Evans POMs presented in **Table 3**. Compounds that contain the $[IMo_6O_{24}]^{5-}$ anion are approximately twice as effective compared to some compounds containing $[Al(OH)_6Mo_6O_{18}]^{3-}$. However, control studies performed with $Na_3[AlMo_6(OH)_6O_{18}] \times 8H_2O$ [200] and $Na_5[IMo_6O_{24}] \times 3H_2O$ [255] have comparable conversion values. Thus, the inorganic Anderson-Evans POM is equal in terms of performance for the photodegradation of RhB without any real need for any further small organic groups to increase the catalytic conversion.

Table 3. The compounds that have been studied for the photodegradation of RhB with UV irradiation. The catalytic conversion is measured as the decrease of the UV signal with time.

Compound	**Catalytic conversion**	**Integrity of catalyst**	**Ref.**
$\{Na_2[(CH_3)_3N(CH_2)_2OH]_4\}[Al(OH)_6Mo_6O_{18}]_2 \times 8NH_2CONH_2 \times 4H_2O$	1 → 0.38 in 360 minutes	No significant loss of reactivity up to four runs.	[193]
$\{[(CH_3)_3N(CH_2)_2OH]_2(H_3O)\}[Na_2(H_2O)_6][IMo_6O_{24}] \times H_2O$	1 → 0.18 in 210 minutes	No significant loss of reactivity up to four runs.	[193]
$[Mn(salen)(H_2O)_2]_2Na_3[IMo_6O_{24}]$	1.6 → 0.1 in 360 minutes	nr*	[255]
$H[(bitdc)Ni(H_2O)_3]_2[IMo_6O_{24}] \times 6H_2O$	1.04 → 0.07 in 11 hours	Conversion of RhB is 97.3%. No changes on the compound after reaction.	[255]
$Mn(salen)_2(H_2O)_2[AlMo_6(OH)_6O_{18}] \times arg \times 20H_2O$	1.2 → 0 in 300 minutes	No significant loss of reactivity up to four runs.	[81]
$Mn(salen)_2(H_2O)_2[CrMo_6(OH)_6O_{18}] \times arg \times 11H_2O$	1.2 → 0.06 in 300 minutes	No significant loss of reactivity up to four runs.	[81]
$\{[Na(arg)_2]NaH\}[AlMo_6(OH)_6O_{18}] \times 6H_2O$	1.4 → 0.4 in 240 minutes	80.67 % conversion of the RhB.	[200]
$H\{CuL_{0.5}^1\ [CrMo_6(OH)_6O_{18}](H_2O)\} \times 0.5L^1$	nr	Degradation ratio of 98.35 %. No changes on the compound after reaction.	[216]
$\{Cu_2(L^2)_2[CrMo_6(OH)_5O_{19}](H_2O)_2\} \times 2H_2O$	nr	Degradation ratio of 99.93 %. No changes on the compound after reaction.	[216]

*nr = not reported a) salen = *N*,*N'*-ethylene-bis(salicylideneiminate, b) bitdc = N,N'-bis(isonicotinoyl)-trans-1,2-diaminocyclohexane, c) arg = *L*-arginine

More sophisticated systems of photocatalysts involving the Anderson-Evans POM have been reported together with porphyrin complexes. Firstly, the porphyrin complexes needs to be connected with hybrid Anderson-Evans POMs hence $Ru^{II}(CO)TPP$ and $Zn^{II}TPP$ were coordinated to the POM since they easily accept one further ligand, such as the nitrogen atom in a pyridine ring (**Figure 17**). However, decomplexation from the Ru center was reported which restricts functional devices [277]. Once the complexation possibilities were investigated, electrochemically generated polymers ($Zn^{II}OEP$) were prepared and used as films (**Figure 12**). The porphyrin in the porphyrin-POM copolymer can act as a photosensitizer able to transfer electrons to the POM upon exposure to visible light. The porphyrin unit would thus be oxidized whereas the POM would be reduced. The reduced POM can transfer one electron to a metal cation to reduce it, whereas a simple reductant such as 2-propanol can reduce the porphyrin, as illustrated in **Figure 17**. This setup proved to be useful in the metal recovery of silver (Ag) where a complete reduction of the Ag^+ occurred and AFM studies on the film after the reaction showed no changes on the morphology. TEM studies revealed formation of silver particles that were inhomogeneous in size and shape [279]. However, when $Zn^{II}TPP$ is used instead of $Zn^{II}OEP$ no electron transfer could be observed onto the Anderson-Evans $Mn^{III}Mo_6$ POM. If the archetype is replaced with a Dawson cluster then electron transfer from the excited porphyrin to the Dawson polyoxometalate is observed again [287], which indicates a rather sensitive system of the Anderson-Evans POM.

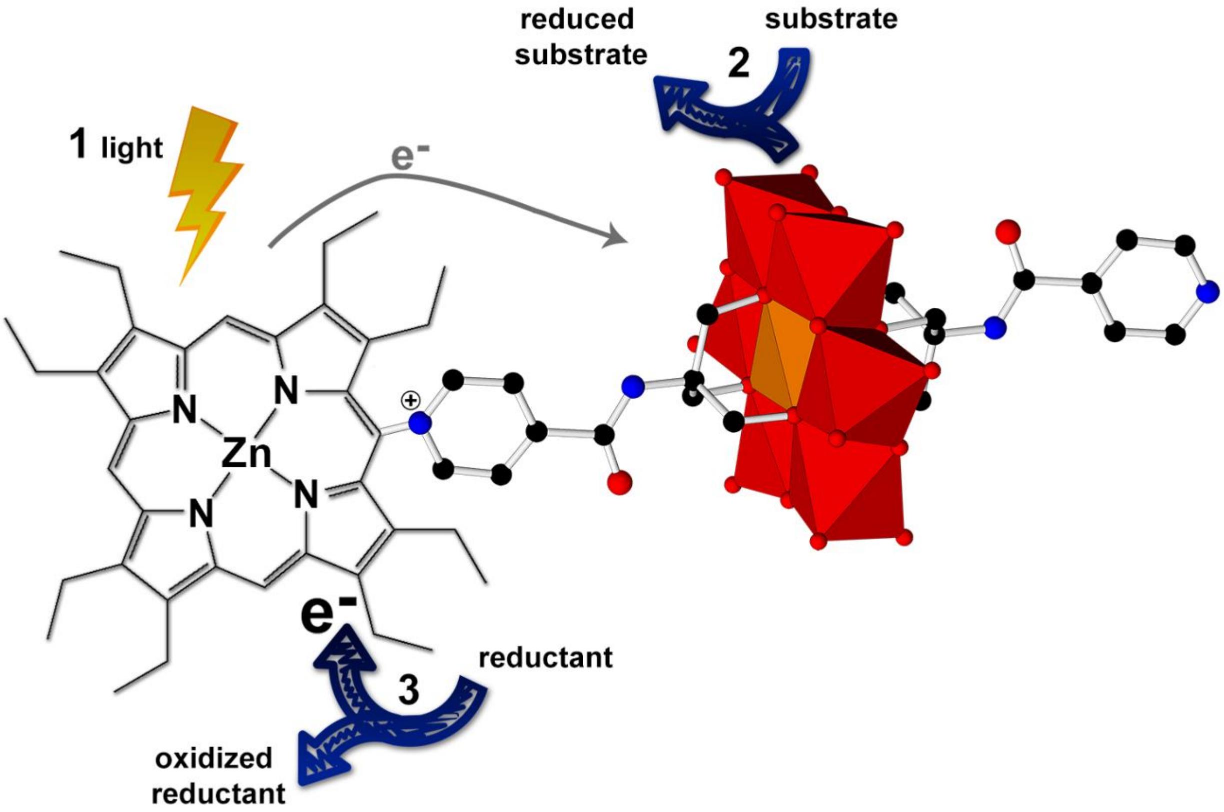

Figure 17. A schematic illustration of complexated ZnOEP-POM (POM = $[MnMo_6O_{18}\{(OCH_2)_3CNHCO(4\text{-}C_5H_4N)\}_2]^{3-}$) which allows transfer of electrons from ZnOEP to the POM (1). The POM can then reduce the substrate (2) and a reductant can reduce back the porphyrin complex (3). Red octahedra: Mo, orange octahedron: Mn; black spheres: C; blue spheres: N; red spheres: O; grey sphere: Zn. Hydrogen atoms are omitted for clarity.

6.4 Magnetic behavior of Anderson-Evans POMs

Design and synthesis of new SMM materials have become a hot topic recently due to their potential applications in high-density information storage and quantum computation [288, 289]. The magnetic behavior in Anderson-Evans POMs comes from heteroatoms in the POM and/or well-defined ligands with polynuclear transition metal clusters. The reports of compounds that exhibit magnetic behavior are reported in **Table 4** and include dinuclear metal centers as the highest nuclearity.

Table 4. Anderson-Evans based compounds exhibiting magnetic properties.

Compound	Magnetic behaviour*	Ref
$(BEDT\text{-}TTF)_4[Cr(OH)_6Mo_6O_{18}] \times 2H_2O$[a]	Paramagnetic S = 3/2 spin originating from Cr^{III}	[211]
$[\{CuTb(sal\text{-}3\text{-}met)(H_2O)_3\}_2\{IMo_6O_{24}\}]Cl \times 2MeOH \times 8H_2O$[b]	SMM behavior from $\{Cu^{II}Tb^{III}\}$	[82]
$[\{CuTb(sal\text{-}3\text{-}met)(H_2O)_2\}_2\{AlMo_6O_{18}(OH)_6\}_2] \times MeOH \times 10H_2O$[b]	SMM behavior from $\{Cu^{II}Tb^{III}\}$	[82]
$[Cu_2(bpy)_2(\mu\text{-}ox)][Al(OH)_7Mo_6O_{17}]$[c]	Antiferromagnetic interactions from $\{Cu^{II}_2\}$	[199]
$[Cu_2(bpy)_2(\mu\text{-}ox)][Cr(OH)_7Mo_6O_{17}]$[c]	Antiferromagnetic interactions from $\{Cu^{II}_2\}$	[199]
$[Ce(H_2O)_7Cr(OH)_6Mo_6O_{18}]_n$	Antiferromagnetic coupled interactions between magnetic centers	[58]
$[Fe(C_5Me_5)_2]_3[Cr(OH)_6Mo_6O_{18}]$	Weak antiferromagentic interactions from	[207]

	$Fe(C_5Me_5)_2^+]_3$	
$Na[Fe(C_5H_5)_2]_2[Cr(OH)_6Mo_6O_{18}]$	Weak antiferromagentic interactions from $Fe(C_5Me_5)_2^+]_3$	[207]
$[\{Ni(pyz)(H_2O)_4\}_2\{CrMo_6(OH)_6O_{18}\}](CH_3COO)_2$ [d]	Weak antiferromagnetic interactions	[210]
$(Hpyz)[\{Co(pyz)_2(H_2O)_2\}\{CrMo_6(OH)_6O_{18}\}]$ [d]	Weak antiferromagnetic interactions	[210]
$(Hpyz)[\{Zn(pyz)_2(H_2O)_2\}\{CrMo_6(OH)_6O_{18}\}]$ [d]	Weak antiferromagnetic interactions	[210]
$(Hpyz)[\{Ni(pyz)_2(H_2O)_2\}\{CrMo_6(OH)_6O_{18}\}]$ [d]	Weak antiferromagnetic interactions	[210]
$[Mn(salen)(H_2O)]_2Na[AlMo_6(OH)_6O_{18}] \times 20H_2O$ [e]	Antiferromagnetic interactions from $\{Mn^{III}_2\}$	[204]
$[Mn(salen)(H_2O)]_2Na[CrMo_6(OH)_6O_{18}] \times 20H_2O$ [e]	Antiferromagnetic interactions from $\{Mn^{III}_2\}$	[199]
$[Cu(phen)]_2[CrMo_6H_5O_{24}]$ [f]	Antiferromagnetic interactions between Cu^{II} complexes. Paramagnetic S = 3/2 spin from Cr^{III}	[173]
(4-*pycH*)$[Gd(H_2O)_4\{CrMo_6(OH)_6O_{18}\}$(4-*pycH*)] [g]	Weak antiferromagnetic interactions	[79]
(4-*pycH*)$_2[Tb(H_2O)_6\{CrMo_6(OH)_6O_{18}\}]$ [g]	Weak antiferromagnetic interactions	[79]
(4-*pycH*)$_2[Sm(H_2O)_6\{CrMo_6(OH)_6O_{18}\}]$ [g]	Weak antiferromagnetic interactions	[79]
$[(3\text{-}Hpya)_2Na][(3\text{-}Hpya)_2Mn(H_2O)_2][CrMo_6H_6O_{24}$ [h]	Weak antiferromagnetic interactions	[56]
$\alpha\text{-}(4\text{-}Hpya)_2\{[(4\text{-}Hpya)_2(H_2O)_3Mn]_2[(H_2O)_4Mn(CrMo_6H_6O_{24})_2]\}$ [i]	Weak antiferromagnetic interactions between spin carriers	[56]
$\beta\text{-}(4\text{-}Hpya)_2[(4\text{-}Hpya)_2(H_2O)_4Mn][CrMo_6H_6O_{24}]\{[(4\text{-}Hpya)(H_2O)_3Mn]_2(CrMo_6H_6O_{24})\}$ [i]	Weak antiferromagnetic interactions between spin carriers	[56]
$[RuNO(en)_2Cl]_3[Cr(OH)_6\ Mo_6O_{18}]_2 \times 17H_2O$ [j]	Paramagnetic S = 3/2 spin originating from Cr^{III}. No observance of paramagnetic Ru^{III}	[65]

*SMM = single-molecule magnet, a) = BEDT-TFF = bis(ethylenedithio)tetrathiafulvalene, b) = sal-3-met = *N*,*N'*-bis(3-methoxysalicylidene)-ethylenediamine, c) = bpy = 2,2'-Bipyridine, d) = pyz = pyrazol, e) = salen = *N*,*N'*-ethylene-bis(salicylideneiminate, f) = phen = 1,10-phenanthroline, g) = 4-*pycH* = 4-pyridinium carboxylate, h) = 3-Hpya = 3-(3-pyridyl)acrylic acid, i) = 4-Hpya = 3-(4-pyridyl)acrylic acid, j) = en = ethylenediamine

The inorganic Anderson-Evans core can incorporate paramagnetic heteroatoms such as Cr^{III} and Fe^{III} which would allow for a long-range order magnetic coupling between localized spins from the transitions metals through the π-electrons in suitable organic ligands which is seen *e.g.* in the compound $(BEDT\text{-}TTF)_4[Cr(OH)_6Mo_6O_{18}] \times 2H_2O$ [211]. The compound $[RuNO(en)_2Cl]_3[Cr(OH)_6Mo_6O_{18}]_2 \times 17H_2O$ also exhibits paramagnetic behavior that indicate non-interacting spins S = 3/2 attributed to Cr^{III} but no indication of a paramagnetic Ru^{III} was observed [65].

Other hybrid structures such as $[\{CuTb(sal\text{-}3\text{-}met)(H_2O)_3\}_2\{IMo_6O_{24}\}]Cl\times2MeOH\times8H_2O$ and $[\{CuTb(sal\text{-}3\text{-}met)(H_2O)_2\}_2\{AlMo_6O_{18}(OH)_6\}_2] \times MeOH \times 10H_2O$ incorporate additional magnetic species forming a dinuclear center. Slow relaxation of the magnetization was observed, which demonstrates SMM behavior, whereas the precursor (sal-3-met), did not exhibited any relaxation. The change of anion from Cl^- to POM modulates the coordination sphere of Tb^{III} enhancing the anisotropy of it and/or shielding of the magnetic interaction by the POMs [82]. A similar behavior has been observed when the Mn-Schiff base compound $[Mn(salen)(H_2O)]_2^{2+}$ was present with $[XMo_6(OH)_6O_{18}]^{3-}$ (X = Al, Cr), which significantly removed the inter-complex antiferromagnetic interactions due to the shielding effect of the $[XMo_6(OH)_6O_{18}]^{3-}$ anion [204].

6.5 Biochemical applications

6.5.1 Macromolecular crystallography

The versatile use of POMs in macromolecular crystallography includes POMs as phasing tools, promoting protein crystallization by stabilizing enzyme conformations, rigidify flexible protein regions and enhancing crystal stability and packing. The highly water soluble Anderson–Evans POM has a very special structure with the average dimensions 8.6 × 8.6 × 2.7 Å which allows positioning of this POM into narrow protein clefts or to migrate through narrow channels inaccessible for larger POM archetypes. The Anderson-Evans POM's high negative charge (e.g. 8^- for MnW_6) is distributed over a large area and can provide crosslinks between monomers with monomer-monomer distances ranging from approximately 5–8 to 11–14 Å. The Anderson-Evans POM $[TeW_6O_{24}]^{6-}$ is stable in the range of pH 4 to 9, which largely covers the pH range at which protein crystallization is normally performed (pH 2 to 10, but predominantly pH 4 to 9). Thus, the Anderson-Evans POM is widely applicable for protein crystallization. Further properties encouraging the use of it in protein crystallization trials are its lack of denaturating or proteolytic effects on proteins and its suitability for hybridization with various organic functionalities to synthesize tailor-made POMs targeting special protein sites [31].

The possibility to decorate inorganic POMs, especially the Anderson-Evans type, with organic moieties opens the door for the synthesis of specifically tailor-made POMs. These POMs could address additional or completely different binding sites on proteins. It is possible to design hybrid-POMs of which focus lies on hydrophobic interactions than on polar ones (which are observed with pure inorganic POMs). This is interesting when it comes to the crystallization of membrane proteins, which is still the real bottleneck in macromolecular crystallography due to their limited solubility. Membrane proteins are obviously underrepresented in the PDB and the usually applied technique to crystallize them is the utilization of detergents in order to decorate their hydrophobic domains. These regions are not approachable by inorganic POMs due to their strong polar character. Therefore, hydrophobically decorated hybrid POMs (**Figure 11D**) could solve this problem and act as a kind of "molecular super detergent". The hybrid POMs could bind hydrophobic membrane protein regions with their hydrophobic site and give them a charged surface by their inorganic POM site leading to a higher solubility, lower flexibility and therefore to a higher amenability for crystal formation.

Recently, the first heterogeneous crystal formation enabled by POM revealed the presence of both the latent and active form of mushroom tyrosinase from *Agaricus bisporus* in one single crystal. The crystals only grew in the presence of the $[TeW_6O_{24}]^{6-}$ anion and the disc-shaped POM was located between two positively charged protein regions of two different monomers coming from adjacent asymmetric units. Thus, the position and interaction of the negatively charged POM led to new crystal contacts, promoting lattice formation and finally the crystal growth (**Figure 18**) [24, 25]. Bijelic et al. reported on the crystallization of $[TeW_6O_{24}]^{6-}$ with the model protein HEWL. The presence of the same anion induced a special crystal packing arrangement leading to a new crystal form. The monomers are cross-linked *via* both the flat side and the long-side of the anion. Thus, the POM allows different binding modes inducing formation of various crystal contacts [23]. These findings might be useful for other proteins that have difficulties with their long-range order arrangement in a crystal lattice.

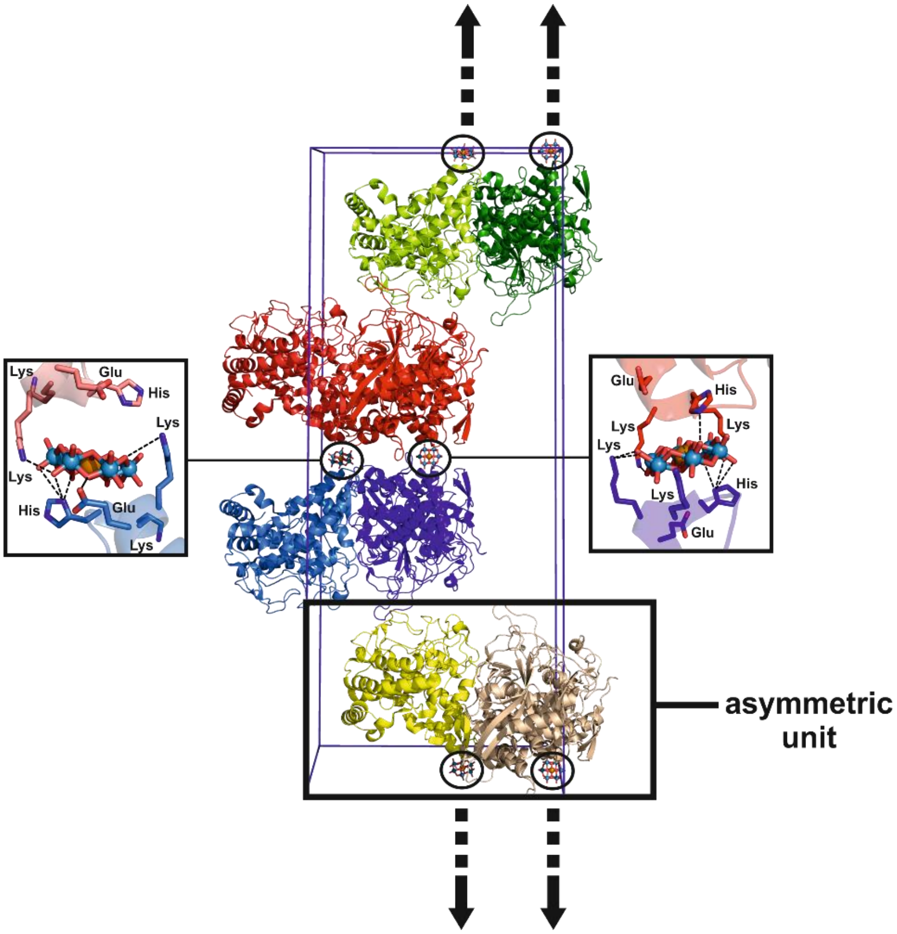

Figure 18. Crystal packing of mushroom tyrosinase PPO4 in a 1 x 2 x 1 supercell. The $[TeW_6O_{24}]^{6-}$ (color code: orange spheres: Te; blue spheres: W; red sticks: O) mediated crosslink between two heterodimers is shown with small insets to the left and right with illustration of the $[TeW_6O_{24}]^{6-}$-protein interactions. PPO4 is demonstrated as cartoon with differently colored protein forms and heterodimers (color code: active form heterodimer 1 = dark red, latent form heterodimer 1 = light red, active form heterodimer 2 = light blue, latent form heterodimer 2 = blue, active form heterodimer 3 = yellow, latent form heterodimer 3 = gold/orange active form heterodimer 4 = light green, latent form heterodimer 4 = dark green). Every heterodimer is connected to two other dimers. The linkage on one side is mediated by two $[TeW_6O_{24}]^{6-}$ anions and on the other site via protein–protein interactions. This motif is repeated throughout the crystal (indicated by arrows), thus demonstrating the role of $[TeW_6O_{24}]^{6-}$ as a form of "glue" between the protein layers.

6.5.2 Bionanomaterials

Song et al. [290] have demonstrated POM-based micro-patterned surfaces for biomolecule or cell interactions. By utilizing micro contact printing the acid 16-mercaptohexadecanoic was stamped on gold surface, with the terminal carboxylic groups directed away from the surface relative to the substrate. Asymmetric (tris-pyrene and tris-NH_2) double-side functionalized $Mn^{III}MO_6$ clusters were coupled to the carboxylic groups *via* their tris-NH_2 functionalities leaving the tris-pyrene side free. Human fibroblasts specifically adhere to the patterned areas containing the aromatic pyrene platforms and control studies on pyrene surfaces in the absence of the POM did not detect any cell adhesion. Thus, the POM is important for the cell response suggesting that the local negative charge and/or the size of the POM cluster might be responsible for the improved cell adhesion. Moreover, it is adhesive onto the POM without the use of any precoated fibronectin [291] or adhesion peptides [292] as previously observed. In conclusion, the anion used for the study demonstrates nicely the advantages with asymmetric functionalization, which is only accessible with the Anderson-Evans POM. This dual functionality makes it an excellent candidate as a biomaterial being able to attach to a surface on one side and offer a different functionality on the opposite side.

6.5.3 Biological activity

6.5.3.1 Antitumor activity

The $[TeW_6O_{24}]^{6-}$ anion was encapsulated in chitosan to enhance the drug carrier properties which was studied against tissue specific calf intestine alkaline phosphatase and tissue non-specific alkaline phosphatase. Increased level of these enzymes may indicate cancer metastasis. The highest activity against tissue non-specific alkaline phosphatase was exhibited by $[TeW_6O_{24}]^{6-}$ (45.4 ± 11.3nM), whereas the nanoassembly of chitosan-$[TeW_6O_{24}]^{6-}$ inhibited tissue specific calf intestine alkaline phosphatase best with K_i value of 22 ± 7nM when compared to $[NaP_5W_{30}O_{110}]^{14-}$ (31.1 ± 7.8nM) and $[V_{10}O_{28}]^{6-}$ (509 ± 17nM) [293]. However, in a larger study with other classical inorganic POMs such as $[H_2W_{12}O_{40}]^{6-}$ and the bigger $[H_7P_8W_{48}O_{184}]^{33-}$, the $[TeW_6O_{24}]^{6-}$ anion exhibited the lowest activity against alkaline phosphatase, which may be due to the presence of the Te atom and the small size of the Anderson-Evans anion compared to the other POM clusters [294]. Similar trends were observed when the cytotoxic potential against HeLa cells was tested. The nanoassembly of chitosan-$[NaP_5W_{30}O_{110}]^{14-}$ containing the significantly bigger anion has the highest percentage of cytotoxicity ($88 \pm 10\%$) in the study [293]. The $[TeW_6O_{24}]^{6-}$ anion was also inactive against human corneal epithelial cells together with all other POM archetypes that were tested but did have satisfactory activity against cancerous H157 [294]. Another compound with the "bent" isomer, $[NH_3Pr^i]_6[Mo_7O_{24}] \times 3H_2O$ was tested *in vivo* against several different tumor cell lines exhibiting potential antitumor activity. The complexation of $[Mo_7O_{24}]^{6-}$ with the biomolecule flavin mononucleotide gives higher redox potential and the robust structure of the POM makes it possible to repeat redox cycles in tumor cells which contributes to the antitumor activity [295]. Thus, the robust structure of the Anderson-Evans POM can contribute to a potential antitumor compound.

6.5.3.2 Antiviral studies

The compound $(NH_4)_{12}H_2(Eu_4(MoO_4)(H_2O)_{16}(Mo_7O_{24})_4) \times 13H_2O$ exhibit potent anti-HIV-1 activity by interfering at an early adsorption and/or penetration step into the cells. It also blocks the replication of simplex virus type 1 and type 2. The potent antiviral properties were attributed to a combination of the presence of Eu and the geometry of the three-dimensional anion structure making the Anderson-Evans POM and interesting candidate [296].

7. Outlook and perspectives

The library of crystals structures containing the Anderson-Evans POM has increased rapidly during the last years. However, many new atoms and molecules remain to be explored within Anderson-Evans

POM based compounds. Several heteroatoms are missing such as Ru and Ag for XMo_6 and XW_6 systems and Cr, Fe, Co, Cu, Pd, Rh for XW_6 systems, which are all in theory accessible [297] and can give rise to a better understanding on the effect of the heteroatom as well as new interesting applications. There are also no reports on tris-functionalized XW_6 systems. A first step towards tris-functionalized XW_6 systems would be to explore new heteroatoms in the XW_6 system that results in B-type Anderson-Evans POMs, which then would allow replacement of the six protons with tris-ligands.

The different synthesis strategies presented herein for tris-functionalized structures have been mastered at a fast paste and it is now possible to *e.g.* simply attach the tris-ligand of choice to an Anderson-Evans cluster instead of going through complicated re-arrangement from other POM archetypes. However, the initial re-arrangement procedure with octamolybdate is still more advantageous in the preparation of larger non-polar tris-ligands. By making small but precise modifications of the cluster at different levels it is possible to synthesize hybrid organic-inorganic anions of high specificity as illustrated in **Figure 7**. The approach may be as simple as changing to more polar solvents in order to obtain single-sided products or refluxing at distinct pH-values to obtain a specific isomer. By being able to control the single-side/double-side attachment as well as where the grafting occurs on the planar surface (δ-isomer or χ-isomer) it is possible to fine tune the accessibility of the heteroatom. Moreover, the unique advantage of the Anderson-Evans cluster also allows straightforward grafting of two tris-ligands due to the planar surface of the Anderson-Evans POM, especially with different properties. The dual functionality of asymmetric grafting gives access to a wide spectrum of applications as demonstrated with numerous examples in chapter 6.

The reports of Anderson-Evans POM compounds with improved magnetic properties may be a direct result of the great challenges associated with increasing nuclearity in the Anderson-Evans archetype. However, this may not be the only approach towards improved magnetic materials as organic molecules that affect crystal packing can significantly modulate magnetic properties. Nevertheless, there are several examples where the Anderson-Evans POM is equal or better than other POM-archetypes. Some Anderson-Evans compounds exhibit photochromic properties with remarkable coloration speeds compared to larger Keggin and Lindqvist structures which originate from its specific geometry. They also make interesting compounds as chromophores toward charge-separated systems in light harvesting devices. The use of the Anderson-Evans POM as an oxidation catalyst gives rise to one of the most efficient POM-photochromic compounds known. Catalysis experiments of water splitting also conclude that the mononuclear heteroatom center in the Anderson-Evans POM is highly active compared to larger POM archetypes exhibiting di- and tetranuclear metal centers. In photocatalytic degradation experiments of RhB Anderson-Evans POMs also exhibit higher conversion values than the Keggin cluster.

Besides photochromic experiments and catalysis, the Anderson-Evans structure is a valuable tool in macromolecular crystallography studies and is far more successful than any other POM archetype, beyond the phasing possibilities. This comes from their specific geometry, usually high water solubility and solution stability. Amphiphillic single-side functionalized POMs makes also interesting candidates as crystallization additives for membrane proteins but the possibility of self-assembly into vesicles makes them suitable as drug-delivery carriers, too. However, out of the Anderson-Evans POMs, only

$[TeW_6O_{24}]^{6-}$ has been investigated so far as crystallization additives. Besides the organic modification and the advantages that they bring, it would still be interesting to investigate *e.g.* heteroatoms in different oxidation states to explore the full potential of the electrostatic interaction. The biological activity of the POMs has also been demonstrated and includes antitumor and antiviral studies which both demonstrate adequate results for further investigations. The studies include only $[TeW_6O_{24}]^{6-}$ and $[Mo_7O_{24}]^{6-}$ and would need to be performed with a greater variety of Anderson-Evans POMs with more biologically relevant heteroatoms as well as hybrid systems containing organically modified tris-ligands with known *e.g.* viral properties whose activity could be enhanced once attached to the POM unit.

In conclusion, the synthesis of the Anderson-Evans POM has been widely explored and the current knowledge could be the key to access new protein structures, materials with interesting properties and efficient catalysts. In some of these cases the realization would be by far suitable only with the Anderson-Evans POM specifically making the Anderson-Evans archetype highly important for future investigations.

8. Acknowledgements

The EU COST Action CM1203 PoCheMoN is highly acknowledged. The authors are truly grateful to Peter Pogacnik for literature research in preparation for this manuscript. We also thank Aleksandar Bijelic, M.Sc. for valuable discussions and critically reading this manuscript.

Abbreviations

3-Hpya = 3-(3-pyridyl)acrylic acid
4-Hpya = 3-(4-pyridyl)acrylic acid
4-*pycH* = 4-pyridinium carboxylate
AFM = atomic force microscopy
OAc = acetate
acac = acetylacetonate
Acn = acetonitrile
arg = *L*-arginine
BEDT-TFF = bis(ethylenedithio)tetrathiafulvalene
bitdc = N,N′-bis(isonicotinoyl)-trans-1,2-diaminocyclohexane
bpy = 2,2'-Bipyridine
DABCO = 1,4-Diazabicyclo[2.2.2]octane
DMF = dimethylformamide
DMSO = dimethylsulfoxide
DODA = dimethyldioctadecyl ammonium
en = ethylenediamine
gly = glycine
HEWL = hen egg white lysozyme
L^1 = *N*,*N*′-bis(3-pyridinecarboxamide)-1,2-ethane
L^2 = *N*,*N*′-bis(3-pyridinecarboxamide)-1.3-propane)
MB = methylene blue
OEP = octaethylporphyrin
PPO4 = polyphenol oxidase 4
pyz = pyrazol

RhB = Rhodamine B
RP-HPLC = reversed-phase high-performance liquid chromatography
sal-3-met = *N*,*N*′-bis(3-methoxysalicylidene)-ethylenediamine
salen = *N*,*N*′-ethylene-bis(salicylideneiminate
salen-am = *N,N′*-bis(salicylideneaminato)ethylene
SMM = single-molecule-magnet
SP = spiropyran, (1-(β-carboxyethyl)-3’,3’-dimethyl-6-nitrospiro(indoline-2’,2[2H-1]benzopyran))
TBA = tetrabutylammonium
TEA = triethanolamine
TEM = transmission electron microscopy
TMA = tetramethylammonium
TPA = tetrapropylammonium
TPP = tetraphenylporphyrin

References

[1] M.T. Pope, Heteropoly and Isopoly Oxometalates, Springer-Verlag, Berlin, 1983.
[2] J.F. Keggin, Nature, 132 (1933) 351-351.
[3] B. Dawson, Acta Crystallogr., 6 (1953) 113-126.
[4] J.S. Anderson, Nature, 140 (1937) 850.
[5] H.T. Evans, J. Am. Chem. Soc., 70 (1948) 1291-1292.
[6] P. Gouzerh, A. Proust, Chem. Rev., 98 (1998) 77-112.
[7] A. Dolbecq, E. Dumas, C.R. Mayer, P. Mialane, Chem. Rev., 110 (2010) 6009-6048.
[8] A. Hiskia, A. Troupis, S. Antonaraki, E. Gkika, P.K.E. Papaconstantinou, Int. J. Environ. Anal. Chem., 86 (2006) 233-242.
[9] A. Müller, R. Sessoli, E. Krickemeyer, H. Bogge, J. Meyer, D. Gatteschi, L. Pardi, J. Westphal, K. Hovemeier, R. Rohlfing, J. Doring, F. Hellweg, C. Beugholt, M. Schmidtmann, Inorg. Chem., 36 (1997) 5239-5250.
[10] A. Rudnitskaya, J.A.F. Gamelas, D.V. Evtuguin, A. Legin, New J. Chem., 36 (2012) 1036-1042.
[11] H.J. Lv, Y.V. Geletii, C.C. Zhao, J.W. Vickers, G.B. Zhu, Z. Luo, J. Song, T.Q. Lian, D.G. Musaev, C.L. Hill, Chem. Soc. Rev., 41 (2012) 7572-7589.
[12] M. Ammam, J. Mat. Chem. A, 1 (2013) 6291-6312.
[13] S.G. Sarafianos, U. Kortz, M.T. Pope, M.J. Modak, Biochemical J., 319 (1996) 619-626.
[14] M. Gluehmann, R. Zarivach, A. Bashan, J. Harms, F. Schluenzen, H. Bartels, I. Agmon, G. Rosenblum, M. Pioletti, T. Auerbach, H. Avila, H.A.S. Hansen, F. Franceschi, A. Yonath, Methods, 25 (2001) 292-302.
[15] K. Stroobants, E. Moelants, H.G.T. Ly, P. Proost, K. Bartik, T.N. Parac-Vogt, Chem. – Eur. J., 19 (2013) 2848-2858.
[16] G. Absillis, R. Van Deun, T.N. Parac-Vogt, Inorg. Chem., 50 (2011) 11552-11560.
[17] J.T. Rhule, C.L. Hill, D.A. Judd, Chem. Rev., 98 (1998) 327-357.
[18] G. Geisberger, S. Paulus, M. Carraro, M. Bonchio, G.R. Patzke, Chem. – Eur. J., 17 (2011) 4619-4625.
[19] T. Yamase, Polyoxometalates Active Against Tumors, Viruses, and Bacteria, in: W.E.G. Müller, X. Wang, H.C. Schröder (Eds.) Biomedical Inorganic Polymers, Springer Berlin Heidelberg, 2013, pp. 65-116.
[20] Z. Ilyas, H.S. Shah, R. Al-Oweini, U. Kortz, J. Iqbal, Metallomics, 6 (2014) 1521-1526.
[21] A. Proust, R. Thouvenot, P. Gouzerh, Chem. Comm., (2008) 1837-1852.
[22] J.M. Clemente-Juan, E. Coronado, A. Gaita-Arino, Chem. Soc. Rev., 41 (2012) 7464-7478.
[23] A. Bijelic, C. Molitor, S.G. Mauracher, R. Al-Oweini, U. Kortz, A. Rompel, ChemBioChem, 16 (2015) 233-241.
[24] S.G. Mauracher, C. Molitor, R. Al-Oweini, U. Kortz, A. Rompel, Acta Crystallogr., Sect D: Biol. Crystallogr., 70 (2014) 2301-2315.

[25] S.G. Mauracher, C. Molitor, R. Al-Oweini, U. Kortz, A. Rompel, Acta Crystallogr., Sect. F: Struct. Biol. Cryst. Commun., 70 (2014) 263-266.
[26] A. Bashan, A. Yonath, J. Mol. Struct., 890 (2008) 289-294.
[27] D. Janell, A. Tocilj, I. Kölln, F. Schlünzen, M. Glühmann, H.S. Hansen, J. Harms, A. Bashan, I. Agmon, H. Bartels, M. Kessler, S. Weinstein, F. Franceshi, A. Yonath, Ribosomal Crystallography and Heteropolytungstates, in: M. Pope, A. Müller (Eds.) Polyoxometalate Chemistry From Topology via Self-Assembly to Applications, Springer Netherlands, 2001, pp. 391-415.
[28] J. Harms, F. Schluenzen, R. Zarivach, A. Bashan, S. Gat, I. Agmon, H. Bartels, F. Franceschi, A. Yonath, Cell, 107 (2001) 679-688.
[29] F. Schluenzen, A. Tocilj, R. Zarivach, J. Harms, M. Gluehmann, D. Janell, A. Bashan, H. Bartels, I. Agmon, F. Franceschi, A. Yonath, Cell, 102 (2000) 615-623.
[30] C. Molitor, S.G. Mauracher, A. Rompel, Acta Crystallogr., Sect. F: Struct. Biol. Cryst. Commun., 71 (2015) 746-751.
[31] A. Bijelic, A. Rompel, Coord. Chem. Rev., 299 (2015) 22-38.
[32] A. Proust, B. Matt, R. Villanneau, G. Guillemot, P. Gouzerh, G. Izzet, Chem. Soc. Rev., 41 (2012) 7605-7622.
[33] D.L. Long, E. Burkholder, L. Cronin, Chem. Soc. Rev., 36 (2007) 105-121.
[34] D.L. Long, R. Tsunashima, L. Cronin, Angew. Chem., Int. Ed. Engl., 49 (2010) 1736-1758.
[35] N.V. Izarova, M.T. Pope, U. Kortz, Angew. Chem., Int. Ed. Engl., 51 (2012) 9492-9510.
[36] D.E. Katsoulis, Chem. Rev., 98 (1998) 359-388.
[37] N. Mizuno, M. Misono, Chem. Rev., 98 (1998) 199-218.
[38] P.A. Lorenzo-Luis, P. Gili, Recent Res. Dev. Inorg. Chem., Vol 2, 2 (2000) 185-196.
[39] M.T. Pope, in: Comprehensive Coordination Chemistry II: From Biology to Nanotechnology, Elsevier Ltd, Oxford, 2004, pp. 635-678.
[40] K.J. Schmidt, G.J. Schrobilgen, J.F. Sawyer, Acta Crystallogr., Sect. C: Cryst. Struct. Commun., 42 (1986) 1115-1118.
[41] H. Kondo, A. Kobayashi, Y. Sasaki, Acta Crystallogr. Sect. B-Struct. Sci., 36 (1980) 661-664.
[42] A. Perloff, Inorg. Chem., 9 (1970) 2228-2239.
[43] C. Wu, X. Lin, R. Yu, W. Yang, C. Lu, H. Zhuang, Sci. China Ser. B, 44 (2001) 49-54.
[44] I. Lindqvist, Acta Crystallogr., 3 (1950) 159-160.
[45] A. Bjornberg, Acta Crystallogr. Sect. B-Struct. Commun., 35 (1979) 1995-1999.
[46] A.M. Nenner, Acta Crystallogr. Sect. C-Cryst. Struct. Commun., 41 (1985) 1703-1707.
[47] C. Livage, E. Dumas, C. Marchal-Roch, G. Hervé, C. r. Acad. sci., Sâer. IIc Chim., 3 (2000) 95-100.
[48] B. Vidyavathy, K. Vidyasagar, Inorg. Chem., 38 (1999) 1394-1400.
[49] B. Vidyavathy, K. Vidyasagar, Inorg. Chem., 37 (1998) 4764-4774.
[50] A.V. Oreshkina, G.Z. Kaziev, S. Holguin Quinones, A.I. Stash, P.A. Shipilova, Russ. J. Coord. Chem., 37 (2011) 845-848.
[51] G.M. Rozantsev, S.V. Radio, N.I. Gumerova, V.N. Baumer, O.B. Shishkin, J. Struct. Chem. , 50 (2009) 296-305.
[52] C.-Y. Sun, S.-X. Liu, L.-H. Xie, C.-L. Wang, B. Gao, C.-D. Zhang, Z.-M. Su, J. Solid State Chem., 179 (2006) 2093-2100.
[53] Y.A. Moroz, A.I. Gruba, M.N. Zayats, L.A. Danileiko, E.V. Dumanova, Zh. Neorg. Khim. , 32 (1987) 927-932.
[54] E.V. Polyakov, T.A. Denisova, L.G. Maksimova, O.I. Gyrdasova, L.I. Manakova, Inorg. Mater. , 38 (2002) 956-961.
[55] K. Nomiya, T. Takahashi, T. Shirai, M. Miwa, Polyhedron, 6 (1987) 213-218.
[56] H. An, X. Liu, H. Chen, Z. Han, H. Zhang, Z. Chen, CrystEngComm, 13 (2011) 5384-5393.
[57] A. Blazevic, E. Al-Sayed, A. Roller, G. Giester, A. Rompel, Chem. - Eur. J., 21 (2015) 4762-4771.

[58] D.-M. Shi, F.-X. Ma, C.-J. Zhang, S. Lu, Y.-G. Chen, Z. Anorg. Allg. Chem. , 634 (2008) 758-763.
[59] L.J. Zhao, S.C. Shen, H.M. Yu, Z. Naturforsch. B Chem. Sci., 63 (2008) 799-803.
[60] S.-M. Wang, Y.-W. Li, X.-J. Feng, Y.-G. Li, E.-B. Wang, Inorg. Chim. Acta, 363 (2010) 1556-1560.
[61] S. Thabet, B. Ayed, A. Haddad, Mater. Res. Bull., 47 (2012) 3791-3796.
[62] V. Shivaiah, T. Chatterjee, S. Das, J. Chem. Sci., 126 (2014) 1525-1533.
[63] L. Yang, Z. Zhou, P.-T. Ma, X.-F. Zhang, J.-P. Wang, J.-Y. Niu, J. Coord. Chem., 66 (2013) 1058-1067.
[64] Q. Gao, F. Li, Y. Wang, L. Xu, J. Bai, Y. Wang, Dalton Trans., 43 (2014) 941-944.
[65] L.A. Kushch, V.A. Emel'yanov, S. Golhen, O. Cador, D. Schaniel, T. Woike, L. Ouahab, E.B. Yagubskii, Inorg. Chim. Acta, 362 (2009) 2279-2282.
[66] H. An, D. Xiao, E. Wang, C. Sun, L. Xu, J. Mol. Struct., 743 (2005) 117-123.
[67] H. An, T. Xu, C. Jia, H. Zheng, W. Mu, J. Mol. Struct., 933 (2009) 86-91.
[68] C.-H. Zhang, C.-J. Zhang, Y.-G. Chen, Solid State Sci., 13 (2011) 1122-1126.
[69] P.-P. Zhang, J. Peng, A.-X. Tian, J.-Q. Sha, H.-J. Pang, Y. Chen, M. Zhu, Y.-H. Wang, J. Mol. Struct., 931 (2009) 50-54.
[70] D. Dutta, A.D. Jana, M. Debnath, A. Bhaumik, J. Marek, M. Ali, Dalton Trans., 39 (2010) 11551-11559.
[71] A.L. Nolan, C.C. Allen, R.C. Burns, D.C. Craig, G.A. Lawrance, ChemInform, 29 (1998) 1.
[72] S.A. Adonin, N.V. Izarova, C. Besson, P.A. Abramov, B. Santiago-Schubel, P. Kogerler, V.P. Fedin, M.N. Sokolov, Chem. Comm., 51 (2015) 1222-1225.
[73] R. Ran, H. Pang, Z. Yu, H. Ma, Y. Xun, J. Coord. Chem., 64 (2011) 2388-2398.
[74] J. Yan, K. Gong, X. Xue, X. He, C. Zhao, Z. Han, H. Yu, Eur. J. Inorg. Chem., 2014 (2014) 5969-5976.
[75] P.A. Lorenzo-Luis, P. Gili, A. Sánchez, E. Rodriguez-Castellón, J. Jiménez-Jiménez, C. Ruiz-Pérez, X. Solans, Transition Met. Chem., 24 (1999) 686-692.
[76] S. Zhang, Y. Li, Y. Liu, R. Cao, C. Sun, H. Ji, S. Liu, J. Mol. Struct., 920 (2009) 284-288.
[77] S. Li, P. Ma, J. Wang, Y. Guo, H. Niu, J. Zhao, J. Niu, CrystEngComm, 12 (2010) 1718-1721.
[78] R. Cao, S. Liu, L. Xie, Y. Pan, J. Cao, Y. Liu, Inorg. Chim. Acta, 361 (2008) 2013-2018.
[79] D. Kumar, S. Ahmad, G.V. Prakash, K.V. Ramanujachary, A. Ramanan, CrystEngComm, 16 (2014) 7097-7105.
[80] H. Naruke, T. Yamase, Acta Crystallogr. Sect. C-Cryst. Struct. Commun., 48 (1992) 597-599.
[81] Q. Wu, W.-L. Chen, D. Liu, C. Liang, Y.-G. Li, S.-W. Lin, E. Wang, Dalton Trans., 40 (2011) 56-61.
[82] X. Feng, W. Zhou, Y. Li, H. Ke, J. Tang, R. Clérac, Y. Wang, Z. Su, E. Wang, Inorg. Chem., 51 (2012) 2722-2724.
[83] P.R. Marcoux, B. Hasenknopf, J. Vaissermann, P. Gouzerh, Eur. J. Inorg. Chem., (2003) 2406-2412.
[84] Y.F. Song, D.L. Long, S.E. Kelly, L. Cronin, Inorg. Chem., 47 (2008) 9137-9139.
[85] C. Yvon, A. Macdonell, S. Buchwald, A.J. Surman, N. Follet, J. Alex, D.-L. Long, L. Cronin, Chem. Sci., 4 (2013) 3810-3817.
[86] B. Hasenknopf, R. Delmont, P. Herson, P. Gouzerh, Eur. J. Inorg. Chem., 2002 (2002) 1081-1087.
[87] H. Evans, Jnr, Acta Crystallogr., Sect. B: Struct. Sci, 30 (1974) 2095-2100.
[88] H.Y. Lee, K.M. Park, U. Lee, H. Ichida, Acta Crystallogr. Sect. C-Cryst. Struct. Commun., 47 (1991) 1959-1961.
[89] V. Shivaiah, P.V. Narasimha Reddy, L. Cronin, S.K. Das, Dalton Trans., (2002) 3781-3782.
[90] S. Manikumari, V. Shivaiah, S.K. Das, Inorg. Chem., 41 (2002) 6953-6955.
[91] C. Martin, C. Lamonier, M. Fournier, O. Mentré, V. Harlé, D. Guillaume, E. Payen, Inorg. Chem., 43 (2004) 4636-4644.
[92] V. Shivaiah, S. Das, J. Chem. Sci., 117 (2005) 227-233.
[93] B. Liu, S. Zhou, C.B. Li, H.G. Zhang, Acta Crystallogr. Sect. E.-Struct Rep. Online, 62 (2006) M3188-M3190.
[94] S. Dhara, S. Dey, S. Basu, M.G.B. Drew, P. Chattopadhyay, Radiochim. Acta, 95 (2007) 297-301.

[95] Y. Zhou, J. Yin, L. Zhang, J. Mol. Str., 920 (2009) 61-67.
[96] G.Z. Kaziev, S.O. Qignones, V.K. Bel'skii, V.E. Zavodnik, I.V. Osminkina, A. de Ita, Russ. J. Inorg. Chem., 47 (2002) 335-340.
[97] H. An, Y. Li, D. Xiao, E. Wang, C. Sun, Cryst. Growth Des., 6 (2006) 1107-1112.
[98] L. Yu, S.-Z. Li, J.-P. Wang, Acta Crystallogr. Sect. E.-Struct Rep. Online, 62 (2006) i190-i192.
[99] D.-P. Zhou, D. Yang, Acta Crystallogr. Sect. E.-Struct Rep. Online, 63 (2007) i113-i115.
[100] L.-Z. Zhang, W. Gu, Z. Dong, X. Liu, B. Li, CrystEngComm, 10 (2008) 1318-1320.
[101] B. Li, L. Ye, L.-X. Wu, Acta Crystallogr. Sect. E: Struct. Rep. Online 67 (2011) i8.
[102] J. Zhang, Z. Zhao, J. Zhang, S. She, Y. Huang, Y. Wei, Dalton Trans., 43 (2014) 17296-17302.
[103] U. Lee, Acta Crystallogr. Sect. E.-Struct Rep. Online, 63 (2007) i5-i7.
[104] H.-C. Joo, K.-M. Park, U. Lee, Acta Crystallogr. Sect. E: Struct. Rep. Online 71 (2015) 157-160.
[105] A.L. Nolan, R.C. Burns, G.A. Lawrance, D.C. Craig, Acta Crystallogr., Sect. C: Cryst. Struct. Commun., 56 (2000) 729-730.
[106] P. Villars, K. Cenzual, J. Daams, R. Gladyshevskii, O. Shcherban, V. Dubenskyy, N. Melnichenko-Koblyuk, O. Pavlyuk, I. Savysyuk, S. Stoyko, L. Sysa, in: P. Villars, K. Cenzual (Eds.) Structure Types. Part 6: Space Groups (166) R-3m - (160) R3m, Springer Berlin Heidelberg, 2008, pp. 50-51.
[107] K. Panneerselvam, M. Soriano-Garcia, S. Holguin-Quinones, E.M. Holt, Acta Crystallogr., Sect. C: Cryst. Struct. Commun., 52 (1996) 1605-1607.
[108] S. M. Garcia, K. Panneerselvam, S.H. Quinones., Anal. Sci., 12 (1996) 535-537.
[109] U. Lee, H.C. Joo, Acta Crystallogr., Sect. C: Cryst. Struct. Commun., 56 (2000) e423-e424.
[110] U. Lee, H.-C. Joo, J.-S. Kwon, M.-A. Cho, Acta Crystallogr. Sect. E: Struct. Rep. Online 57 (2001) i112-i114.
[111] G.Z. Kaziev, A.A. Dutov, S.H. Quinones, V.K. Bel'skij, V.E. Zavodnik, A. Delta, Russ. J. Inorg. Chem., 48 (2003) 972-976.
[112] S.H. Quinones, G.Z. Kaziev, A. V. Oreshkina, V. E. Zavodnik, R. M. Rodriguez, S. L. A. Sanches, Russ. J. Inorg. Chem., 50 (2005) 1696-1701.
[113] A.L. Nolan, R.C. Burns, G.A. Lawrance, Dalton Trans., (1996) 2629-2636.
[114] F.-X. Liu, C. Marchal-Roch, D. Dambournet, A. Acker, J. Marrot, F. Sécheresse, Eur. J. Inorg. Chem., 13 (2008) 2191-2198.
[115] U. Lee, H.-C. Joo, J.-S. Kwon, Acta Crystallogr. Sect. E: Struct. Rep. Online 58 (2002) i6-i8.
[116] B. Liu, L. Feng, S. Zhou, C.-B. Li, W. Zhou, Acta Crystallogr. Sect. E: Struct. Rep. Online 63 (2007) i14-i15.
[117] F. Ito, T. Ozeki, H. Ichida, H. Miyamae, Y. Sasaki, Acta Crystallogr., Sect. C: Cryst. Struct. Commun., 45 (1989) 946-947.
[118] C.C. Allen, R.C. Burns, G.A. Lawrance, P. Turner, T.W. Hambley, Acta Crystallogr., Sect. C: Cryst. Struct. Commun., 53 (1997) 7-9.
[119] Z.L. Mensinger, L.N. Zakharov, D.W. Johnson, Acta Crystallogr. Sect. E: Struct. Rep. Online 64 (2008) i8-i9.
[120] S. Himeno, S. Murata, K. Eda, Dalton Trans., (2009) 6114-6119.
[121] H.T. Evans, B.M. Gatehouse, P. Leverett, Dalton Trans., (1975) 505-514.
[122] E. Shimao, Bull. Chem. Soc. Jpn., 40 (1967) 1609-1613.
[123] U. Kortz, M.T. Pope, Acta Crystallogr., Sect. C: Cryst. Struct. Commun., 51 (1995) 1717-1719.
[124] Z.I. Khazheeva, E.G. Khaikina, K.M. Khal'baeva, T.A. Shibanova, V.N. Molchanov, V.I. Simonov, Crystallogr. Rep., 45 (2000) 916-918.
[125] J.J. Cruywagen, M.W. Esterhuysen, J.B.B. Heyns, Inorg. Chim. Acta, 348 (2003) 205-211.
[126] Q.-L. Chen, R.-H. Zhang, Z.-H. Zhou, H.-L. Wan, Inorg. Chem. Commun., 13 (2010) 1366-1369.
[127] L. Hao, J. Chen, X. Zhang, Acta Crystallogr. Sect. E: Struct. Rep. Online 66 (2010) i34-i35.

[128] Y. Ozawa, Y. Hayashi, K. Isobe, Acta Crystallogr., Sect. C: Cryst. Struct. Commun., 47 (1991) 637-638.
[129] G.Z. Kaziev, S.O. Quignones, V.K. Bel'skii, V.E. Zavodnik, I.V. Osminkina, Russ. J. Inorg. Chem., 47 (2002) 14-18.
[130] S. Angus-Dunne, Robert C. Burns, Donald C. Craig, Geoffrey A. Lawrance, Z. Anorg. Allg. Chem., 636 (2010) 727-734.
[131] A. Ogawa, H. Yamato, U. Lee, H. Ichida, A. Kobayashi, Y. Sasaki, Acta Crystallogr., Sect. C: Cryst. Struct. Commun., 44 (1988) 1879-1881.
[132] U.K. Lee, Y. Sasaki, Bull. Korean Chem. Soc., 8 (1987) 1-3.
[133] C. Robl, M. Frost, Z. Anorg. Allg. Chem., 619 (1993) 1834-1840.
[134] C. Robl, M. Frost, Z. Anorg. Allg. Chem., 619 (1993) 1137-1146.
[135] C. Robl, M. Frost, Z. Anorg. Allg. Chem., 619 (1993) 1624-1628.
[136] B. Gao, S.X. Liu, C.D. Zhang, L.H. Xie, C.Y. Sun, M. Yu, J. Coord. Chem., 60 (2007) 911-918.
[137] C. Robl, M. Frost, Z. Naturforsch. B Chem. Sci., 48 (1993) 404-408.
[138] C. Robl, M. Frost, Z. Anorg. Allg. Chem. , 619 (1993) 1132-1136.
[139] P.A. Lorenzo-Luis, P. Martin-Zarza, P. Gili, R.S. Puche, J. Jimenez-Jimenez, E. Rodriguez-Castellon, C. Ruiz-Perez, J. Gonzalez-Platas, X. Solans, Eur. J. Solid State Inorg. Chem., 34 (1997) 1259-1271.
[140] D. Drewes, E. M. Limanski, B. Krebs, Eur. J. Inorg. Chem., 2004 (2004) 4849-4853.
[141] D. Drewes, E.M. Limanski, B. Krebs, Dalton Trans., (2004) 2087-2091.
[142] D. Drewes, B. Krebs, Z. Anorg. Allg. Chem. , 631 (2005) 2591-2594.
[143] M.S. Grigor'ev, Y.T. Struchkov, A.M. Fedoseev, A.B. Yusov, A.I. Yanovskii, Zh. Neorg. Khim. , 37 (1992) 2507-2514.
[144] I.A. Charushnikova, A.M. Fedoseev, A.B. Yusov, C. Den Auwer, Crystallogr. Rep., 50 (2005) 191-193.
[145] B. Gao, S.-X. Liu, L.-H. Xie, M. Yu, C.-D. Zhang, C.-Y. Sun, H.-Y. Cheng, J. Solid State Chem., 179 (2006) 1681-1689.
[146] X.H. Yan, S.F. Mo, Z.H. Ju, J.G. Wu, K.L. Yao, Synth. React. Inorg. Met.-Org. Chem., 38 (2008) 529-533.
[147] Y. Liu, S.-X. Liu, R.-G. Cao, H.-M. Ji, S.-W. Zhang, Y.-H. Ren, J. Solid State Chem., 181 (2008) 2237-2242.
[148] C. Rosu, T.J.R. Weakley, Acta Crystallogr. Sect. C-Cryst. Struct. Commun., 56 (2000) E170-E171.
[149] H. An, E. Wang, D. Xiao, Y. Li, L. Xu, Inorg. Chem. Comm., 8 (2005) 267-270.
[150] K.G. Burtseva, T.S. Chernaya, M.I. Sirota, Dokl. Phys., 23 (1978) 784-786.

[151] E.O. Tolkacheva, V.S. Sergienko, A.B. Ilyukhin, S.V. Meshkov, Zh. Neorg. Khim. , 42 (1997) 752-764.
[152] U. Lee, Y. Sasaki, Chem. Lett., 13 (1984) 1297-1300.
[153] U. Lee, A. Kobayashi, Y. Sasaki, Acta Crystallogr. Sect. C-Cryst. Struct. Commun., 39 (1983) 817-819.
[154] U. Lee, Bull. Korean Chem. Soc., 9 (1988) 256-257.
[155] U. Lee, H. Ichida, A. Kobayashi, Y. Sasaki, Acta Crystallogr. Sect. C-Cryst. Struct. Commun., 40 (1984) 5-7.
[156] K.M. Park, U. Lee, Chem. Lett., 18 (1989) 1943-1946.
[157] U. Lee, Y. Sasaki, Taehan Hwahakhoe Chi, 31 (1987) 118-120.
[158] U. Lee, Acta Crystallogr. Sect. C-Cryst. Struct. Commun., 50 (1994) 1657-1659.
[159] U. Lee, H.-C. Joo, Acta Crystallogr. Sect. E: Struct. Rep. Online, 62 (2006) i241-i243.
[160] U. Lee, Acta Crystallogr. Sect. E: Struct. Rep. Online, 58 (2002) i130-i132.
[161] U. Lee, H.C. Joo, Acta Crystallogr. Sect. C-Cryst. Struct. Commun., 56 (2000) e311-e312.
[162] U. Lee, H.-C. Joo, Acta Crystallographica Section E, 60 (2004) i61-i63.
[163] U. Lee, H.-C. Joo, Acta Crystallogr. Sect. E: Struct. Rep. Online, 60 (2004) i86-i88.
[164] U. Lee, H.-C. Joo, Acta Crystallogr. Sect. E: Struct. Rep. Online, 63 (2007) i11-i13.

[165] U. Lee, H.-C. Joo, K.-M. Park, Acta Crystallogr. Sect. E: Struct. Rep. Online, 60 (2004) i55-i57.
[166] U. Lee, H.-C. Joo, Acta Crystallogr. Sect. E: Struct. Rep. Online, 62 (2006) i231-i233.
[167] U. Lee, H.-C. Joo, Acta Crystallogr. Sect. E: Struct. Rep. Online, 66 (2010) i8-i9.
[168] U. Lee, H.-C. Joo, Acta Crystallogr. Sect. E: Struct. Rep. Online, 60 (2004) i33-i36.
[169] U. Lee, H.-C. Joo, K.-M. Park, Acta Crystallogr. Sect. E: Struct. Rep. Online, 66 (2010) i25.
[170] H.-Y. Wang, C.-J. Zhang, C.-H. Zhang, Q. Tang, Y.-G. Chen, J. Coord. Chem., 64 (2011) 1481-1490.
[171] C.-G. Lin, W. Chen, D.-L. Long, L. Cronin, Y.-F. Song, Dalton Trans., 43 (2014) 8587-8590.
[172] G. Yan, X. Wang, Y. Ma, X. Cheng, Y. Wang, Y. Li, Solid State Sci., 17 (2013) 146-150.
[173] H.-y. Ma, L.-z. Wu, H.-j. Pang, X. Meng, J. Peng, J. Mol. Struct., 967 (2010) 15-19.
[174] Q. Wu, Q.X. Han, L.J. Chen, P.T. Ma, J.Y. Niu, Z.Naturforsch.(B), 65 (2010) 163-167.
[175] J. Li, L.C. Zhang, Z.G. Sun, C.H. Tian, Z.M. Zhu, Y. Zhao, Y.Y. Zhu, J. Zhang, N. Zhang, L. Liu, X. Lu, Z. Anorg. Allg. Chem., 634 (2008) 1173-1176.
[176] K. Pavani, A. Ramanan, Eur. J. Inorg. Chem., 2005 (2005) 3080-3087.
[177] W. Zhang, J. Gong, L. Zhang, Y. Yang, Y. Liu, H. Zhang, G. Zhang, H. Dong, H. Hu, F. Zhao, Z. Kang, Dalton Trans., 42 (2013) 1760-1769.
[178] M.H. Rosnes, C. Yvon, D.-L. Long, L. Cronin, Dalton Trans., 41 (2012) 10071-10079.
[179] J. Fuchs, H. Hartl, Angew. Chem.-Int. Edit. Engl., 15 (1976) 375-376.
[180] I. Lindqvist, Arkiv for Kemi, 2 (1950) 349-355.
[181] Y.-F. Song, D.-L. Long, L. Cronin, Angew. Chem., Int. Ed. Engl., 46 (2007) 3900-3904.
[182] M.H. Rosnes, C. Musumeci, C. Yvon, A. Macdonell, C.P. Pradeep, C. Sartorio, D.-L. Long, B. Pignataro, L. Cronin, Small, 9 (2013) 2316-2324.
[183] M.H. Rosnes, C. Musumeci, C.P. Pradeep, J.S. Mathieson, D.-L. Long, Y.-F. Song, B. Pignataro, R. Cogdell, L. Cronin, J. Am. Chem. Soc., 132 (2010) 15490-15492.
[184] Y.-F. Song, D.-L. Long, S.E. Kelly, L. Cronin, Inorg. Chem., 47 (2008) 9137-9139.
[185] O. Oms, K. Hakouk, R. Dessapt, P. Deniard, S. Jobic, A. Dolbecq, T. Palacin, L. Nadjo, B. Keita, J. Marrot, P. Mialane, Chem. Comm., 48 (2012) 12103-12105.
[186] B. Zhang, L. Yue, Y. Wang, Y. Yang, L. Wu, Chem. Comm., 50 (2014) 10823-10826.
[187] P. Wu, P. Yin, J. Zhang, J. Hao, Z. Xiao, Y. Wei, Chem. - Eur. J., 17 (2011) 12002-12005.
[188] J. Zhang, J. Luo, P. Wang, B. Ding, Y. Huang, Z. Zhao, J. Zhang, Y. Wei, Inorg. Chem., 54 (2015) 2551-2559.
[189] J. Zhang, Y. Huang, J. Zhang, S. She, J. Hao, Y. Wei, Dalton Trans., 43 (2014) 2722-2725.
[190] Y. Ji, J. Hu, L. Huang, W. Chen, C. Streb, Y.-F. Song, Chem. - Eur. J., 21 (2015) 6469-6474.
[191] R.-G. Cao, S.-X. Liu, Y. Liu, Q. Tang, L. Wang, L.-H. Xie, Z.-M. Su, J. Solid State Chem., 182 (2009) 49-54.
[192] X.-D. Yang, Y.-G. Chen, M. Mirzaei, A.R. Salimi, F. Yao, Inorg. Chem. Comm., 12 (2009) 195-197.
[193] S.-M. Wang, W.-L. Chen, E.-B. Wang, Y.-G. Li, X.-J. Feng, L. Liu, Inorg. Chem. Comm., 13 (2010) 972-975.
[194] R.K. Tan, S.X. Liu, W. Zhang, S.J. Li, Y.Y. Zhang, Inorg. Chem. Comm., 14 (2011) 384-388.
[195] P.-P. Zhang, J. Peng, A.-X. Tian, H.-J. Pang, Y. Chen, M. Zhu, D.-D. Wang, M.-G. Liu, Y.-H. Wang, J. Coord. Chem., 63 (2010) 3610-3619.
[196] J.-P. Wang, J.-W. Zhao, S.-Z. Li, J.-Y. Niu, J. Coord. Chem., 59 (2006) 597-605.
[197] J.-P. Wang, S.-Z. Li, J.-Y. Niu, J. Coord. Chem., 60 (2007) 1327-1334.
[198] F. Wang, R.-G. Cao, Y.-B. Pan, S.-X. Liu, Acta Crystallogr. Sect. E: Struct. Rep. Online 64 (2008) m1069-m1070.
[199] R. Cao, S. Liu, L. Xie, Y. Pan, J. Cao, Y. Ren, L. Xu, Inorg. Chem., 46 (2007) 3541-3547.
[200] S.W. Lin, Q. Wu, E.B. Wang, Chem. Res. Chin. Univ., 28 (2012) 375-378.
[201] V. Shivaiah, S.K. Das, Inorg. Chem., 44 (2005) 8846-8854.
[202] V. Shivaiah, M. Nagaraju, S.K. Das, Inorg. Chem., 42 (2003) 6604-6606.

[203] V. Shivaiah, T. Chatterjee, K. Srinivasu, S.K. Das, Eur. J. Inorg. Chem., 2 (2007) 231-234.
[204] Q. Wu, Y.-G. Li, Y.-H. Wang, R. Clerac, Y. Lu, E.-B. Wang, Chem. Comm., 38 (2009) 5743-5745.
[205] Y. Hu, H. An, X. Liu, J. Yin, H. Wang, H. Zhang, L. Wang, Dalton Trans., 43 (2014) 2488-2498.
[206] K. Pavani, M. Singh, A. Ramanan, Aust. J. Chem., 64 (2011) 68-76.
[207] S. Golhen, L. Ouahab, D. Grandjean, P. Molinié, Inorg. Chem., 37 (1998) 1499-1506.
[208] Y.-Y. Yang, Y. Song, L.-Y. Liu, X.-S. Qu, Acta Crystallogr. Sect. E: Struct. Rep. Online 67 (2011) m776.
[209] M. Singh, A. Ramanan, Cryst. Growth Des., 11 (2011) 3381-3394.
[210] M. Singh, S.E. Lofland, K.V. Ramanujachary, A. Ramanan, Cryst. Growth Des., 10 (2010) 5105-5112.
[211] L. Ouahab, S. Golhen, Y. Yoshida, G. Saito, J. Cluster Sci., 14 (2003) 193-204.
[212] F. Yao, Y.-G. Chen, A. Salimi, M. Mirzaei, J. Cluster Sci., 22 (2011) 309-318.
[213] A.S.J. Wery, J.M. Gutierrez-Zorrilla, A. Luque, M. Ugalde, P. Roman, L. Lezama, T. Rojo, ChemInform, 30 (1999).
[214] H. An, Y. Li, E. Wang, D. Xiao, C. Sun, L. Xu, Inorg. Chem., 44 (2005) 6062-6070.
[215] M. Singh, D. Kumar, A. Ramanan, Proc. Natl. Acad. Sci., India, Sect. A, 84 (2014) 305-314.
[216] X. Wang, Z. Chang, H. Lin, A. Tian, G. Liu, J. Zhang, D. Liu, RSC Adv., 5 (2015) 14020-14026.
[217] A. Saad, G. Rousseau, H. El Moll, O. Oms, P. Mialane, J. Marrot, L. Parent, I.-M. Mbomekallé, R. Dessapt, A. Dolbecq, J. Cluster Sci., 25 (2014) 795-809.
[218] B. Liu, S. Zhou, C.B. Li, H.G. Zhang, Acta Crystallogr. Sect. E.-Struct Rep. Online, 62 (2006) M3185-M3187.
[219] H. Liu, L. Xu, Acta Crystallogr. Sect. E.-Struct Rep. Online, 63 (2007) m872-m874.
[220] Y.Y. Yang, L. Xu, F.Y. Li, X.S. Qu, Inorg. Chem. Commun., 33 (2013) 142-146.
[221] Q.L. He, E.B. Wang, Inorg. Chim. Acta, 295 (1999) 244-247.
[222] J. Iijima, H. Naruke, H. Takiyama, Acta crystallographica. Section E, Structure reports online, 69 (2013) m612-613.
[223] U. Lee, S.J. Jang, H.C. Joo, K.M. Park, Acta Crystallogr. Sect. E.-Struct Rep. Online, 59 (2003) M345-M347.
[224] R.M. Dessapt, M. Gabard, M. Bujoli-Doeuff, P. Deniard, S.p. Jobic, Inorg. Chem., 50 (2011) 8790-8796.
[225] Q.L. He, E.B. Wang, Inorg. Chem. Commun., 2 (1999) 399-402.
[226] F.Y. Su, B.B. Zhou, Z.F. Zhao, Z.H. Su, C.C. Zhu, Cryst. Res. Technol., 44 (2009) 447-452.
[227] M.D. Liu, Z.H. Su, Y.C. Shang, Acta Crystallogr. Sect. E.-Struct Rep. Online, 66 (2010) M1308-U1270.
[228] L.L. Li, B. Liu, G.L. Xue, H.M. Hu, F. Fu, J.W. Wang, Cryst. Growth Des., 9 (2009) 5206-5212.
[229] J.Y. Niu, J.A. Hua, X. Ma, J.P. Wang, Crystengcomm, 14 (2012) 4060-4067.
[230] C.Y. Sun, Y.G. Li, E.B. Wang, D.R. Xiao, H.Y. An, L. Xu, Inorg. Chem., 46 (2007) 1563-1574.
[231] W. Kwak, L.M. Rajkovic, J.K. Stalick, M.T. Pope, C.O. Quicksall, Inorg. Chem., 15 (1976) 2778-2783.
[232] E. Burkholder, S. Wright, V. Golub, C.J. O'Connor, J. Zubieta, Inorg. Chem., 42 (2003) 7460-7471.
[233] Y. Ohashi, K. Yanagi, Y. Sasada, T. Yamase, Bull. Chem. Soc. Jpn., 55 (1982) 1254-1260.
[234] P. Román, J. Gutiérrez-Zorrilla, M. Martínez-Ripoll, S. García-Blanco, Transition Met. Chem., 11 (1986) 143-150.
[235] H. Liu, H. Wang, D. Niu, Z. Lu, Synth. React. Inorg. Met.-Org. Chem., 37 (2007) 103-107.
[236] T. Arumuganathan, A.S. Rao, S.K. Das, Cryst. Growth Des., 10 (2010) 4272-4284.
[237] K. Heussner, M. Grabau, J. Forster, C. Streb, Eur. J. Inorg. Chem., 2011 (2011) 5125-5131.
[238] P. Román, J.M. Gutiérrez-Zorrilla, A. Luque, M. Martínez-Ripoll, J. Crystallogr. Spectrosc. Res., 18 (1988) 117-131.
[239] A. Don, T.J.R. Weakley, Acta Crystallogr., Sect. B: Struct. Sci., 37 (1981) 451-453.
[240] P. Roman, A. San Jose, A. Luque, J.M. Gutierrez-Zorrilla, Acta Crystallogr., Sect. C: Cryst. Struct. Commun., 50 (1994) 1031-1034.

[241] P. Gili, P.A. Lorenzo-Luis, A. Mederos, J.M. Arrieta, G. Germain, A. Castiñeiras, R. Carballo, Inorg. Chim. Acta, 295 (1999) 106-114.
[242] A. Wutkowski, B.R. Srinivasan, A.R. Naik, C. Schütt, C. Näther, W. Bensch, Eur. J. Inorg. Chem., 2011 (2011) 2254-2263.
[243] V. Coué, R. Dessapt, M. Bujoli-Doeuff, M. Evain, S. Jobic, Inorg. Chem., 46 (2007) 2824-2835.
[244] P. Roman, A. Luque, A. Aranzabe, J.M. Gutierrez-Zorrilla, Polyhedron, 11 (1992) 2027-2038.
[245] J.-Y. Niu, X.-Z. You, T.C.W. Mak, Z.-Y. Zhou, Polyhedron, 15 (1996) 519-525.
[246] P. Gili, P.A. Lorenzo-Luis, P. Martin-Zarza, S. Dominguez, A. Sanchez, J.M. Arrieta, E. Rodriguez-Castellon, J. Jimenez-Jimenez, C. Ruiz-Perez, M. Hernandez-Molina, X. Solans, Transition Met. Chem., 24 (1999) 141-151.
[247] M. Ali, D. Dutta, S. Biswas, J. Marek, A.D. Jana, Crystengcomm, 11 (2009) 2608-2610.
[248] F. Wang, S.-X. Liu, C.-L. Wang, R.-G. Cao, J.-F. Cao, Acta Crystallogr. Sect. E: Struct. Rep. Online, 63 (2007) m1708-m1709.
[249] Y. Liu, S. Liu, H. Ji, S. Zhang, L. Cai, R. Cao, J. Cluster Sci., 20 (2009) 535-543.
[250] Z.-h. Xu, P.-x. Xi, F.-j. Chen, Z.-z. Zeng, Anal. Sci.: X-Ray Struct. Anal. Online, 23 (2007) x235-x236.
[251] S. Mo, Z. Ju, Z. Xu, J. Wu, K. Yao, Synth. React. Inorg. Met.-Org. Chem., 36 (2006) 687-692.
[252] J. Kang, J. Ahn, H. Shin, S. Pyo, H. Yun, J. Do, Z. Kristallogr. - New Cryst. Struct., 226 (2011) 129-130.
[253] Z.-h. Xu, X.-f. Li, X.-w. Zhang, Synth. React. Inorg. Met.-Org. Chem., 42 (2012) 140-144.
[254] Q. Wu, S.-W. Lin, Y.-G. Li, E.-B. Wang, Inorg. Chim. Acta, 382 (2012) 139-145.
[255] H. Chen, H. An, X. Liu, H. Wang, Z. Chen, H. Zhang, Y. Hu, Inorg. Chem. Commun., 21 (2012) 65-68.
[256] H. An, Y. Li, E. Wang, J. Coord. Chem., 59 (2006) 379-387.
[257] D. Honda, S. Ikegami, T. Inoue, T. Ozeki, A. Yagasaki, Inorg. Chem., 46 (2007) 1464-1470.
[258] J. Fuchs, E.P. Flindt, Z. Naturforsch. B Chem. Sci., 34 (1979) 412-422.
[259] V.W. Day, J.C. Goloboy, W.G. Klemperer, Eur. J. Inorg. Chem., 2009 (2009) 5079-5087.
[260] S. Ikegami, K. Kani, T. Ozeki, A. Yagasaki, Chem. Comm., 46 (2010) 785-787.
[261] U. Lee, S.-J. Jang, H.-C. Joo, K.-M. Park, Acta Crystallogr. Sect. E: Struct. Rep. Online, 59 (2003) m116-m118.
[262] H. Ai, Y. Wang, B. Li, L. Wu, Eur. J. Inorg. Chem., 2014 (2014) 2766-2772.
[263] Pierre R. Marcoux, B. Hasenknopf, J. Vaissermann, P. Gouzerh, Eur. J. Inorg. Chem., 2003 (2003) 2406-2412.
[264] S. Favette, B. Hasenknopf, J. Vaissermann, P. Gouzerh, C. Roux, Chem. Comm., (2003) 2664-2665.
[265] C.-M. Liu, Y.-H. Huang, D.-Q. Zhang, S. Gao, F.-C. Jiang, J.-Y. Zhang, D.-B. Zhu, Cryst. Growth Des., 5 (2005) 1531-1538.
[266] Y.-F. Song, H. Abbas, C. Ritchie, N. McMillian, D.-L. Long, N. Gadegaard, L. Cronin, J. Mater. Chem., 17 (2007) 1903-1908.
[267] Y.-F. Song, N. McMillan, D.-L. Long, J. Thiel, Y. Ding, H. Chen, N. Gadegaard, L. Cronin, Chem. - Eur. J., 14 (2008) 2349-2354.
[268] Y.-F. Song, D.-L. Long, L. Cronin, CrystEngComm, 12 (2010) 109-115.
[269] J. Zhang, J. Hao, Y. Wei, F. Xiao, P. Yin, L. Wang, J. Am. Chem. Soc., 132 (2010) 14-15.
[270] M.-P. Santoni, A.K. Pal, G.S. Hanan, A. Proust, B. Hasenknopf, Inorg. Chem., 50 (2011) 6737-6745.
[271] J. Thiel, D. Yang, M.H. Rosnes, X. Liu, C. Yvon, S.E. Kelly, Y.-F. Song, D.-L. Long, L. Cronin, Angew. Chem., Int. Ed. Engl., 50 (2011) 8871-8875.
[272] J. Zhang, P. Yin, J. Hao, F. Xiao, L. Chen, Y. Wei, Chem. - Eur. J., 18 (2012) 13596-13599.
[273] Z. He, Y. Yan, B. Li, H. Ai, H. Wang, H. Li, L. Wu, Dalton Trans., 41 (2012) 10043-10051.
[274] Y. Yan, B. Li, Q. He, Z. He, H. Ai, H. Wang, Z. Yin, L. Wu, Soft Matter, 8 (2012) 1593-1600.
[275] M. Hutin, C. Yvon, J. Yan, A. Macdonell, D.-L. Long, L. Cronin, CrystEngComm, 15 (2013) 4422-4430.
[276] C. Yvon, A.J. Surman, M. Hutin, J. Alex, B.O. Smith, D.-L. Long, L. Cronin, Angew. Chem., Int. Ed. Engl., 126 (2014) 3404-3409.

[277] C. Allain, S. Favette, L.-M. Chamoreau, J. Vaissermann, L. Ruhlmann, B. Hasenknopf, Eur. J. Inorg. Chem., 2008 (2008) 3433-3441.
[278] A. Macdonell, N.A.B. Johnson, A.J. Surman, L. Cronin, J. Am. Chem. Soc., 137 (2015) 5662-5665.
[279] D. Schaming, C. Allain, R. Farha, M. Goldmann, S. Lobstein, A. Giraudeau, B. Hasenknopf, L. Ruhlmann, Langmuir, 26 (2010) 5101-5109.
[280] J. Zhang, Y.-F. Song, L. Cronin, T. Liu, J. Am. Chem. Soc., 130 (2008) 14408-14409.
[281] R. Pardo, M. Zayat, D. Levy, Chem. Soc. Rev., 40 (2011) 672-687.
[282] K. Hakouk, O. Oms, A. Dolbecq, J. Marrot, A. Saad, P. Mialane, H. El Bekkachi, S. Jobic, P. Deniard, R. Dessapt, J. Mater. Chem. C, 2 (2014) 1628-1641.
[283] S.S. Bayraq, A. Nikseresht, I. Khosravi, Phosphorus, Sulfur Silicon Relat. Elem, 188 (2012) 1236-1243.
[284] S. Tanaka, M. Annaka, K. Sakai, Chem. Comm., 48 (2012) 1653-1655.
[285] X. Chen, Z. Xue, Y. Yao, W. Wang, F. Zhu, C. Hong, Int. J. Photoenergy, 2012 (2012) 5.
[286] C.C. Chen, W. Zhao, P.X. Lei, J.C. Zhao, N. Serponer, Chem. - Eur. J., 10 (2004) 1956-1965.
[287] C. Allain, D. Schaming, N. Karakostas, M. Erard, J.-P. Gisselbrecht, S. Sorgues, I. Lampre, L. Ruhlmann, B. Hasenknopf, Dalton Trans., 42 (2013) 2745-2754.
[288] M.N. Leuenberger, D. Loss, Nature, 410 (2001) 789-793.
[289] J. Lehmann, A. Gaita-Arino, E. Coronado, D. Loss, Nat. Nanotechnol., 2 (2007) 312-317.
[290] Y.-F. Song, N. McMillan, D.-L. Long, S. Kane, J. Malm, M.O. Riehle, C.P. Pradeep, N. Gadegaard, L. Cronin, J. Am. Chem. Soc., 131 (2009) 1340-1341.
[291] S. Aota, M. Nomizu, K.M. Yamada, J. Biol. Chem., 269 (1994) 24756-24761.
[292] S.P. Massia, J.A. Hubbell, J. Cell Biol., 114 (1991) 1089-1100.
[293] H.S. Shah, R. Al-Oweini, A. Haider, U. Kortz, J. Iqbal, Toxicol. Rep., 1 (2014) 341-352.
[294] R. Raza, A. Matin, S. Sarwar, M. Barsukova-Stuckart, M. Ibrahim, U. Kortz, J. Iqbal, Dalton Trans., 41 (2012) 14329-14336.
[295] T. Yamase, Mol. Eng., 3 (1993) 241-262.
[296] Y. Inouye, Y. Tokutake, T. Yoshida, Y. Seto, H. Hujita, K. Dan, A. Yamamoto, S. Nishiya, T. Yamase, S. Nakamura, Antiviral Res., 20 (1993) 317-331.
[297] M. Pope, A. Müller, Polyoxometalate Chemistry From Topology via Self-Assembly to Applications, Springer, 2001.